Novel insights into the factors influencing rhizosphere reactive oxygen species production and their role in polycyclic aromatic hydrocarbons transformation

Jinbo Liu, Siqi Shen, Kecheng Zhu, Ziyan Li, Na Chen, Eric Lichtfouse, Hanzhong Jia

Soil Biology and Biochemistry 198 (2024) 109562

https://doi.org/10.1016/j.soilbio.2024.109562

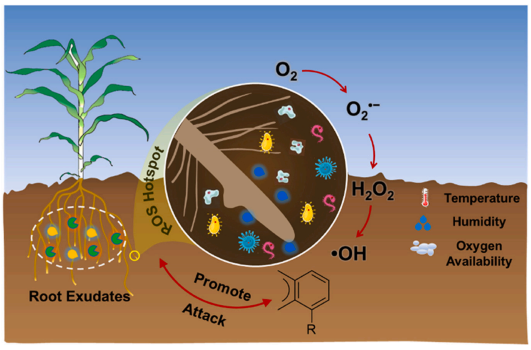

Novel insights into the factors influencing rhizosphere reactive oxygen species production and their role in polycyclic aromatic hydrocarbons transformation

Jinbo Liu [a,b], Siqi Shen [a], Kecheng Zhu [a], Ziyan Li [a], Na Chen [a], Eric Lichtfouse [c], Hanzhong Jia [a,*]

[a] Key Laboratory of Low-carbon Green Agriculture in Northwestern China, Ministry of Agriculture and Rural Affairs, College of Natural Resources and Environment, Northwest A&F University, Yangling, 712100, China
[b] School of Petroleum Engineering and Environmental Engineering, Yan'an University, Yan'an, 716000, China
[c] International Research Center for Renewable Energy, State Key Laboratory of Multiphase Flow in Power Engineering, Xi'an Jiaotong University, Xi'an, 710049, China

Keywords:
Reactive oxygen species (ROS)
Rhizosphere
Root development
Environmental conditions
Polycyclic aromatic hydrocarbons (PAHs)

A B S T R A C T

Reactive oxygen species (ROS) are recognised as pivotal biogeochemical process drivers. However, the factors influencing ROS production in the rhizosphere and their role in pollutant transformation remain elusive. We investigated ROS with a focus on spatiotemporal variations in superoxide radicals ($O_2^{\bullet-}$), hydrogen peroxide (H_2O_2), and hydroxyl radicals ($^{\bullet}OH$) in the rhizosphere of maize during root development, and elucidated the impact of environmental conditions on ROS production. *In-situ* visualisation by fluorescence imaging showed that ROS hotspots gradually shifted from seminal to lateral roots during maize growth, indicating that newly developed roots are the major contributors to ROS production. The three types of ROS contents changed with root growth, suggesting that root development regulates ROS production. The ROS contents reached a maximum at 25 °C and 45% maximum field capacity. Both ambient temperature and soil moisture indirectly influenced ROS production by regulating the release of root exudates to induce changes in water-soluble phenols and dissolved organic carbon (DOC). In contrast, ROS content gradually increased with oxygen availability, which directly mediated ROS generation by acting as a precursor. More interestingly, the presence of polycyclic aromatic hydrocarbons (PAHs) significantly enhanced ROS generation, which further promoted PAH removal with a contribution of 31.4–43.3%. These findings provide new insights into the occurrence, distribution, and environmental effects of ROS in the rhizosphere.

1. Introduction

Reactive oxygen species (ROS), such as superoxide radicals ($O_2^{\bullet-}$), hydrogen peroxide (H_2O_2), and hydroxyl radicals ($^{\bullet}OH$), occur ubiquitously in various environmental media (Gligorovski et al., 2015; Hayyan et al., 2016; Guo et al., 2023), and contribute to carbon turnover, elemental cycling, pollutant transformation, and the regulation of physiological functions in organisms (Mopper and Zhou, 1990; Trusiak et al., 2018). ROS are typically produced by photolytic reactions involving organic photosensitisers such as natural organic matter (Yan et al., 2021), black carbon (Wang et al., 2023), and inorganic compounds such as iron minerals and nitrate (Trusiak et al., 2018; Zheng et al., 2023). In addition to the well-known photolytic production of ROS, several studies have established ROS generation via redox processes under dark ambient conditions, such as in aphotic freshwater (Vermilyea et al., 2010), deep oceans (Wu et al., 2015; Roe et al., 2016), and subsurfaces (Page et al., 2013; Trusiak et al., 2018; Zhang et al., 2020). Recently, the soil rhizosphere has become a new "hotspot" for ROS generation. ROS generation was found in the rhizosphere of rice due to interaction between microbial respiration interaction, which discharged extracellular electrons, and dioxygen released by the roots (Dai et al., 2022). Our recent research also reported that combined biotic and abiotic processes, including microbial community-driven extracellular superoxide radical ($O_2^{\bullet-}$) release, Fe(II)/Fe(III) cycling, and Fe(II) and water-soluble phenol-mediated electron transfer, induced ROS production in the rhizosphere of ryegrass (Liu et al., 2022a). Therefore, it is reasonable to speculate that ROS hotspots are ubiquitous in the rhizospheres of both aquatic and terrestrial plants. To promote scientific

* Corresponding author.
E-mail address: jiahz@nwafu.edu.cn (H. Jia).

progress in understanding soil biogeochemical processes, it is important to gain information on ROS generation, distribution, and environmental impacts in the rhizosphere.

The rhizosphere is a complex interface with intensive biogeochemical processes induced by the roots (Kuzyakov and Razavi, 2019). Compared with bulk soil, the rhizosphere is characterised by unique pH values, higher amounts of organic substances, enzymatic activity, and microbial abundance (Gunina and Kuzyakov, 2015; Liu et al., 2020, 2022b). These characteristics are influenced by intrinsic plant growth factors such as root development (primary, secondary, and tertiary roots), which alters the zonation and constituents of exudates being released. For example, sucrose is predominantly exuded from the apical region of the primary root, whereas efflux of the amino acid tryptophan is linked to branch roots (Jaeger et al., 1999). On the other hand, rhizosphere characteristics are influenced by external abiotic factors such as temperature, soil moisture, and oxygen availability. For example, elevated soil temperatures can stimulate microbial activity and boost the membrane permeability of root cells, thereby enhancing enzymatic activity and expediting exudate release (Razavi et al., 2016). ROS production is closely related to physicochemical and biological rhizosphere properties (Liu et al., 2022a). However, limited studies have been conducted to explain how rhizosphere properties, which are influenced by root development and environmental conditions, affect ROS generation. This knowledge gap hinders a comprehensive assessment of the environmental implications of rhizosphere ROS under natural conditions.

ROS play critical roles in mediating organic pollutant redox transformations owing to their high reactivity (Manning et al., 2005; Guo et al., 2022). Particularly, hydroxyl radicals ($^{\bullet}OH$, standard reduction potential: 2.8 V (Wardman, 1989)) is the most powerful oxidant in natural systems, which can unselectively oxidise most organic substrates (Tong et al., 2016; Yu and Kuzyakov, 2021). For example, $^{\bullet}OH$ produced by the oxygenation of anoxic paddy slurries efficiently degrades polycyclic aromatic hydrocarbons (PAHs) through hydroxylation and ring opening (Chen et al., 2021). Therefore, in the rhizosphere, the reaction of organic pollutants with ROS represents a new mechanism for contaminated soil phytoremediation. However, the contribution of ROS to rhizosphere pollutant transformation remains unclear, and the associated remediation mechanisms are gaps in the current understanding.

In the current study, maize, a plant extensively used for PAH remediation (Yoshitomi and Shann, 2001; Khan et al., 2014), was used to examine potential ROS generation in the rhizosphere. The primary objectives were (i) to probe the spatiotemporal variation of ROS ($O_2^{\bullet-}$, H_2O_2, and $^{\bullet}OH$) during root development; (ii) to elucidate the effects of environmental conditions (soil moisture, temperature, and oxygen availability) on rhizosphere ROS production and its corresponding mechanisms, and (iii) to assess the contribution of rhizosphere ROS to the transformation of various PAH molecules (naphthalene - NAP, anthracene - ANT, and phenanthrene - PHE).

2. Materials and methods

2.1. Chemicals and soil samples

Detailed information regarding the chemicals used in this study can be found in Supporting Information SI1. The Lou soil (Eum-Orthic Anthrosol, USDA) was collected from the upper layer (0− 20 cm) of the cultivated fields located in Shaanxi Province (34°17′ N, 108°01′ E) in China. The soil samples were dried naturally at room temperature and subsequently sieved through a 2 mm mesh prior to analyses and batch experiments. The soil physicochemical properties were analysed as described in our previous study (Liu et al., 2022a). The analysis methods are described in SI2. The pH, cation exchange capacity and organic carbon were 8.67, 37.73 cmol kg^{-1} and 9.58 g kg^{-1}, respectively. The soil clay, silt, and sand contents were 12.79, 55.43, and 31.78%, respectively. The soil Fe, Mn, Cu, Zn and Ni contents were 16347.42, 237.91, 0.49, 6.87 and 5.46 mg kg^{-1}, respectively.

2.2. Microcosm experiment

The spatial evolution of ROS during root development was characterised *in situ* using ROS-trapping technology. Specifically, maize (*Zea mays* L.) was cultivated in a rhizobox (length × width × depth, 100 × 50 × 150 mm; Fig. S1), which was placed at an angle of approximately 45° to ensure that the roots clung to the inner wall because of gravitational force. Considering spatial constraints in the experimental setup, it was not feasible to implement *in-situ* visualisation of ROS throughout the life cycle of maize. After cultivating for predetermined intervals (1, 5, 9, 13, 17 and 35 d), ROS characterisation was performed using a 2′,7′-dichlorodihydrofluorescein diacetate (DCFH-DA) substrate, which can react with ROS, generating 2′,7′-dichlorofluorescein (DCF) with fluorescent characteristics (Lebel et al., 1992). Briefly, DCFH-DA was dissolved in phosphate-buffered saline (10 mM, pH 7.0) at a concentration of 2 μM. Subsequently, the substrate with water was sprayed onto the soil surface attached to the inner wall. After incubating the soil saturated with DCFH-DA in the dark for 1 h, it was placed under a multispectral dynamic fluorescence microscopic imaging system (PlantView100; Guangzhou Boluteng Instrument Co., Ltd., China) to capture optimal fluorescence images (Fig. S2). The PlantView100 specific operating parameters were a sample length of 155 mm, sample height of 5 mm, exposure time of 0.1 s; excitation wavelength of 480 nm, emission wavelength of 520 nm, and lamp source of 90%. To investigate the changes in ROS hotspots, we defined ROS hotspots with reference to the enzymatic activity hotspots (Razavi et al., 2016). Specifically, DCF fluorescence was transferred into 16-bit greyscale using ImageJ, with correction for environmental variations and camera noise. The calibration equation obtained for ROS was used to convert the fluorescence pixel grey values into the ROS content. ROS content exceeding 25% of the mean corresponding content of the entire soil was defined as a hotspot.

2.3. Batch experiments

2.3.1. Evolution of rhizosphere ROS with maize growth

Variations in ROS, including $O_2^{\bullet-}$, H_2O_2, and $^{\bullet}OH$, with maize growth were explored to clarify the effect of root development on ROS generation at a temporal scale using a pot experiment. Briefly, soil (500 g) was placed in plastic pots (length × width × depth: 30 × 20 × 15 cm). Subsequently, two evenly-sized maize seeds were sown in the pots after sterilisation with 3% H_2O_2. After germination, the seedlings were thinned to one plant per pot and pre-incubated for 7 d to promote root growth. Finally, the maize was placed in a natural greenhouse at Northwest A&F University. To maintain soil moisture at approximately 60% of the maximum field capacity, deionised water was periodically added throughout the 90 d cultivation period. At specific intervals (0, 1, 2, 3, 4, 5, 6, 9, 12, 15, 18, 24, 30, 36, 45, 54, 63, 72, 81, and 90 d), a batch incubation experiment (five replicates × 20 sampling times = 100 pots total) was conducted. The soil adhering to the roots after shaking was considered as rhizosphere soil (Courchesne and Gobran, 1997), which was obtained by scraping off the attached soil. Non-rhizosphere soil was used as a control. The soil samples obtained were immediately used for analysis of ROS content and physicochemical properties.

2.3.2. Generation of rhizosphere ROS under different environmental conditions

Rhizosphere ROS content was quantitatively determined using chemical probes during maize growth at different temperatures. Maize seeds were germinated on filter paper under dark conditions for 3 d. One seedling was then transplanted into a plastic pot containing 500 g of soil. Subsequently, the pots were placed in a climate chamber under a controlled culturing temperature of 15 ± 1, 20 ± 1, 25 ± 1, 30 ± 1 and 35 ± 1 °C and a daily light period of 16 h with an illumination intensity

of 10000 lx. Distilled water was periodically added during maize growth to maintain soil moisture at approximately 60% of the maximum field capacity. As the concentrations of $O_2^{\bullet-}$ and H_2O_2 reached their highest and stable levels at 24 d, as observed in the pre-experiment, the batch incubation experiment was sacrificed after 24 d of cultivation. Subsequent procedures were consistent with those described in the pot experiments. The influence of soil moisture on rhizosphere ROS generation was investigated by following the same steps described above except the soil water content was maintained at 15, 30, 45, 60, 75 and 90% of the maximum field capacity through periodic irrigation, and the cultivation temperature was controlled at 20 ± 1 °C.

The effects of oxygen availability on rhizosphere ROS generation were investigated using a rhizobox. Briefly, different soil weights were used to fill a rhizobox (length × width × depth, 100 × 50 × 150 mm) with a volume of 750 cm^3 to achieve different diffusivity coefficients of oxygen (DC_o) in the rhizosphere, according to the protocol of Nakhaie et al. (2020). The specific method is provided in SI3, and the soil weight and oxygen availability settings are listed in Table S1. Subsequently, one maize seedling was transplanted into a rhizobox, and the samples were placed in a climate chamber with a controlled temperature of 20 ± 1 °C. During maize growth, the soil moisture content was maintained at 20% through periodic watering. The remaining procedures were similar to those described above.

2.3.3. Transformation of PAHs in the rhizosphere

A detailed method for the preparation of PAH-contaminated soils is provided in SI4. The influence of rhizosphere ROS on PAH transformation was investigated following the same steps described above in the context of temperature effects. At preselected intervals (7, 14, 21, and 28 d), a batch incubation experiment was sacrificed, and the rhizosphere soil was collected for ROS and PAH determination. The extraction and measurement methods for PAHs are described in SI5. Moreover, to further explore the role of ROS in PAH transformation, coumarin (0.12 mg g^{-1}) and *p*-benzoquinone (0.16 mg g^{-1}) were added to PAH-contaminated soil before planting maize (Jia et al., 2015). This dosage of scavengers had a notable inhibitory effect on ROS (Fig. S3) while exerting a negligible impact on plant growth (Fig. S4). After incubation for 28 d, the rhizosphere soils were collected, and PAH residual concentrations were determined using high-performance liquid chromatography (Thermo Fisher Scientific U3000).

2.4. ROS quantitation

Different chemical probes were used to quantitatively determine the ROS content. Briefly, the $O_2^{\bullet-}$ content was determined using 2,3-bis(2-methoxy-4-nitro-5-sulfophenyl)-2Htetrazolium-5-carboxanilide (XTT), which reacts with $O_2^{\bullet-}$ to produce XTT formazan (Fu et al., 2016). H_2O_2 content was detected using a hydrogen peroxide assay kit. Benzoic acid was used to measure the content of $^{\bullet}OH$ according to its reaction with $^{\bullet}OH$ to generate 4-hydroxybenzoic acid (Zhang and Yuan, 2017). Detailed procedures for determining $O_2^{\bullet-}$, H_2O_2, and $^{\bullet}OH$ are provided in SI6.

2.5. Measurement of rhizosphere soil physicochemical and biological properties

The contents of water-soluble phenols, Fe(II), and dissolved organic carbon (DOC) in the rhizosphere soil were analysed, and detailed procedures are provided in SI7–SI9. The maize root exudates incubated for different intervals (0, 9, 24, 54, 72, and 90 d) and cultivated under different environmental conditions were measured; the specific procedures are presented in SI10. In addition, enzymatic activity related to microbial activity (urease and dehydrogenase) and ROS-related enzymes, such as catalase, were determined (SI11). The rhizosphere soils under different environmental conditions were collected to analyze bacterial 16S rDNA genes by amplicon sequencing (SI12).

2.6. Statistical analysis

Data are expressed as mean ± standard deviation of five replicates. Significant differences in testing indices among the different groups were evaluated using one-way analysis of variance, followed by the LSD test. Correlation analysis was performed using Origin 2022 to explore the pivotal factors related to ROS production. Subsequently, structural equation modelling (SEM) was applied to elucidate the potential pathways for ROS production using Amos software (version 20.0; IBM Corporation Software Group, Somers, NY, USA).

3. Results

3.1. ROS evolution with root development

Higher fluorescence intensity was observed at the root–soil interface (Fig. 1), suggesting ROS generation in the maize rhizosphere. In addition, the proportion of ROS hotspots in the root zone profile initially increased and then decreased with maize growth, reaching a maximum of 17.3% on day 17. Interestingly, the ROS hotspots were mostly in the seminal roots at the early stage of cultivation, however, ROS exhibited stronger fluorescence intensity in the lateral roots during incubation.

To gain a deeper understanding of ROS formation in the rhizosphere, the contents of the three representative ROS ($O_2^{\bullet-}$, H_2O_2 and $^{\bullet}OH$) during root growth were quantified. Three types of ROS were detected in the non-rhizosphere soils, however, the changes in their concentrations with maize growth were not obvious (Fig. S5). Comparatively, the ROS content in the rhizosphere soils was 3–15 times higher than that in the non-rhizosphere soils, displaying noticeable variations during maize growth. Specifically, the $O_2^{\bullet-}$ content gradually increased during the initial 24 d of incubation (Fig. S5a). Subsequently, the $O_2^{\bullet-}$ concentration gradually declined and returned to its initial level after 90 d of cultivation. Similarly, the H_2O_2 content followed a trend comparable to that of $O_2^{\bullet-}$, reaching a peak on day 24 of cultivation (Fig. S5b). In contrast to $O_2^{\bullet-}$ and H_2O_2, the $^{\bullet}OH$ content reached its maximum after pre-incubation and then gradually decreased with maize growth (Fig. S5c).

3.2. Changes of rhizosphere ROS under different environmental conditions

The influence of culture temperature on the ROS content in the rhizosphere was pronounced (Fig. 2). Specifically, the $O_2^{\bullet-}$ content first increased and then decreased with an increase in culture temperature, reaching a maximum of 23.17 μM kg^{-1} at 25 °C (Fig. 2a). Similarly, the H_2O_2 and $^{\bullet}OH$ contents also displayed a comparable pattern with that of $O_2^{\bullet-}$, reaching a maximum of 19.24 and 9.13 μM kg^{-1} at 25 °C, respectively (Fig. 2b–c). In terms of biomass, there was no difference in root length under different temperature conditions, ranging from 19.3 to 20.9 cm (Fig. S9a). In contrast, the stem length of maize varied under different temperature conditions (Fig. S9b). Briefly, the stem length first increased and then decreased with temperature, reaching a maximum of 65.1 cm at 25 °C.

Except for the soil sample with moisture at 90% of the maximum field capacity that inhibited root length (Fig. S10a), negligible effects on maize root length were observed under other soil moisture conditions. In contrast, the difference in soil moisture induced a change in maize stem length (Fig. S10b). When the soil moisture increased from 15 to 45%, the stem length reached a maximum of 66.7 cm, and then decreased. The $O_2^{\bullet-}$ content first increased and then decreased with increasing soil moisture, reaching a maximum at 45% (Fig. 2d). The H_2O_2 and $^{\bullet}OH$ contents also displayed a pattern similar to that of $O_2^{\bullet-}$, attaining a maximum at 45% (Fig. 2e–f).

A prominent difference in rhizosphere ROS content was observed at different DC_o (Fig. 2g–i). Specifically, the $O_2^{\bullet-}$ content gradually increased with the increase in DC_o, reaching a maximum at 8.97 m^2 10^6

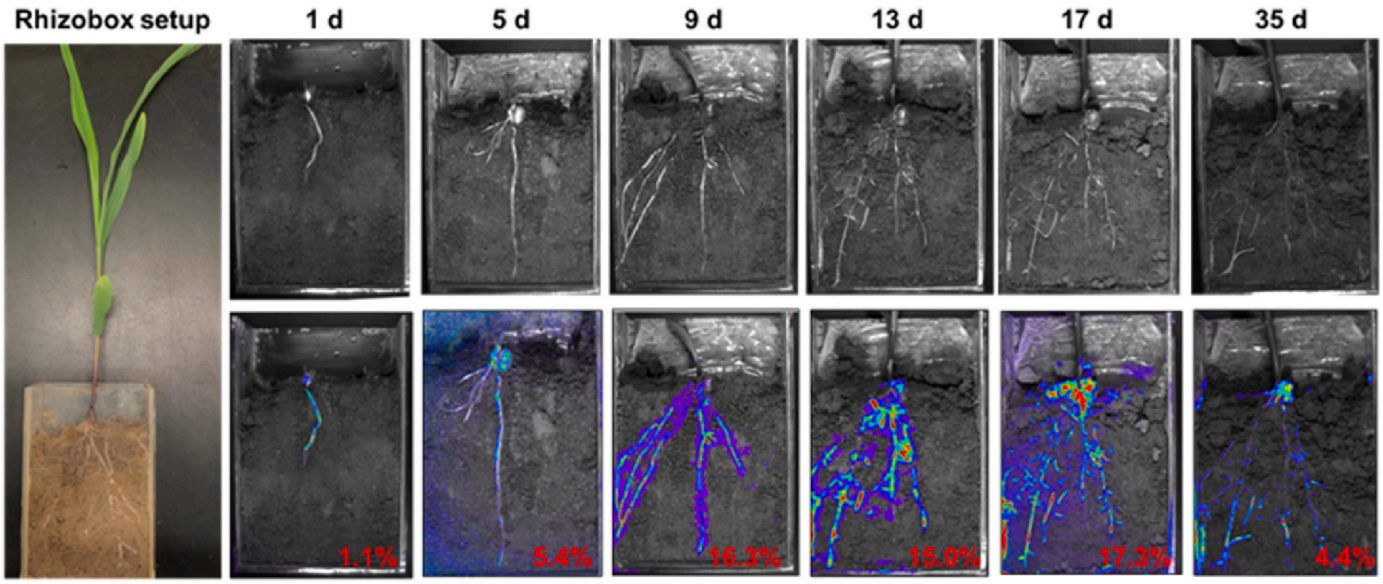

Fig. 1. Accumulation of ROS in the rhizosphere of maize. The corresponding fluorescence imaging displayed the hotspot of ROS generation in the root-soil interface at different incubation times, and the red number in the bottom right corner of the picture represented the proportion of ROS hotspots.

s^{-1} (Fig. 2g). The H_2O_2 and $^{\bullet}OH$ contents also showed a comparable trend with $O_2^{\bullet-}$, attaining a maximum at 8.97 m^2 10^6 s^{-1} (Fig. 2h–i). Compared to temperature and soil moisture, both root and stem lengths were influenced by oxygen availability (Fig. S11).

3.3. Evolution of root exudates, enzymatic activity, bacterial abundance and redox components

The types of compounds in the root exudates were essentially equivalent, however, the total abundance of the compounds first increased and then decreased with incubation (Fig. S6a). Moreover, the urease, dehydrogenase, and catalase activity in the rhizosphere soils displayed a similar trend to that in the root exudates (Figs. S6b–d). Briefly, urease and dehydrogenase activity, commonly indicative of microbial activity (Pascual et al., 1998), exhibited a rapid increase over time, reaching a peak at 24 d, and then gradually returning to the initial level as incubation progressed (Figs. S6b–c). Catalase activity, associated with ROS generation and decay in soil (Shi et al., 2021), also displayed a similar time-dependent pattern as those of urease and dehydrogenase, attaining a peak of 2.48 mg H_2O_2 g^{-1} 20 min^{-1} at 15 d (Fig. S6d). Moreover, water-soluble phenols, a component of root exudates, also increased during the first 24 d of incubation and then decreased thereafter (Fig. S7c). However, the Fe(II) and DOC concentrations exhibited different trends (Figs. S7a–b). The Fe(II) content decreased before day 24, reaching an equilibrium of approximately 10.14 mg kg^{-1} (Fig. S7a). A comparable pattern was also found for the variation in the DOC content (Fig. S7b).

There was no obvious difference in Fe(II) content under different temperatures (Fig. S12a), maintaining a constant level of 30.57–32.78 mg kg^{-1}. Comparatively, the temperature had an obvious influence on the DOC content (Fig. S12b). Briefly, the DOC content first increased and then decreased with temperature, reaching a maximum of 58.67 mg kg^{-1} at 25 °C. Simultaneously, the water-soluble phenol content displayed a similar pattern to that of DOC, attaining a maximum of 16.98 μg g^{-1} at 25 °C (Fig. S12c). The catalase activity also changed significantly with temperature (Fig. S12d), reaching a maximum at 25 °C. Compared with catalase activity, urease activity gradually increased with increasing temperature, with the highest activity 3.51 mg NH_4–N g^{-1} 24 h^{-1} at 35 °C (Fig. S12e). Additionally, the root exudate content first increased and then decreased with increasing temperature, reaching a maximum at 25 °C (Fig. S12f). Furthermore, soil bacterial 16S rDNA gene sequencing results revealed that Actinobacteria, Proteobacteria, Acidobacteria, Actinobacteria, Chloroflexi, and Bacteroidota, were the dominant bacterial phyla in rhizosphere soil incubated at various temperatures (Fig. S13), and the relative abundance of dominant bacterial phyla increased with temperature.

At different soil moisture conditions, the Fe(II) content increased with increasing soil moisture, reaching a maximum at 90% (Fig. S14a). Comparatively, the DOC and water-soluble phenol contents first increased and then decreased with soil moisture, reaching a maximum at 45% (Figs. S14b–c). Moreover, both catalase and urease activity first increased and then decreased with soil moisture, reaching their maxima at 45 and 60%, respectively (Figs. S14d–e). In addition, root exudate content increased and then decreased with increasing soil moisture, reaching a maximum at 45%, particularly for organic acids (Fig. S14f). In contrast, the influence of soil moisture on dominant bacterial phyla abundance was negligible (Fig. S15).

The different oxygen availabilities exhibited no significant differences in the DOC levels (Fig. S16b), water-soluble phenols (Fig. S16c), root exudates (Fig. S16f), and bacterial abundance (Fig. S17). Specifically, the DOC and water-soluble phenol contents under different DC_o remained at a constant level, ranging from 50.21 to 51.47 mg kg^{-1} and 12.52–13.43 μg g^{-1}, respectively (Figs. S16b–c). The relative abundance of dominant bacterial phyla also remained in the range of 78.1–79.9% under different DC_o levels (Fig. S17). Moreover, the changing trends in the Fe(II) content and urease activity differred from those of the ROS (Figs. S16a and S16e). Briefly, the Fe(II) content decreased with the increase in DC_o, reaching a minimum when the DC_o was 8.97 m^2 10^6 s^{-1} (Fig. S16a), whereas urease activity first increased and then decreased with DC_o, reaching a maximum at 4.81 m^2 10^6 s^{-1} (Fig. S16e).

3.4. Rhizosphere ROS changes in the presence of PAHs

Along with incubation (7–28 d), both $O_2^{\bullet-}$ and H_2O_2 contents in PAH-contaminated rhizosphere soils gradually increased, whereas the $^{\bullet}OH$ concentration slightly decreased, exhibiting a trend similar to that of rhizosphere soil without PAHs (Fig. 4). Notably, all PAHs (NAP, PHE, and ANT) promoted ROS production at 14, 21, and 28 d, particularly ANT. For example, the $O_2^{\bullet-}$, H_2O_2, and $^{\bullet}OH$ contents in rhizosphere soil without PAH addition were 4.58, 3.76 and 4.91 μM kg^{-1}, respectively, at 14 d. In the presence of NAP, PHE, and ANT, the $O_2^{\bullet-}$, H_2O_2, and $^{\bullet}OH$ contents in rhizosphere soils increased to 5.37, 4.18 and 5.09 μM kg^{-1},

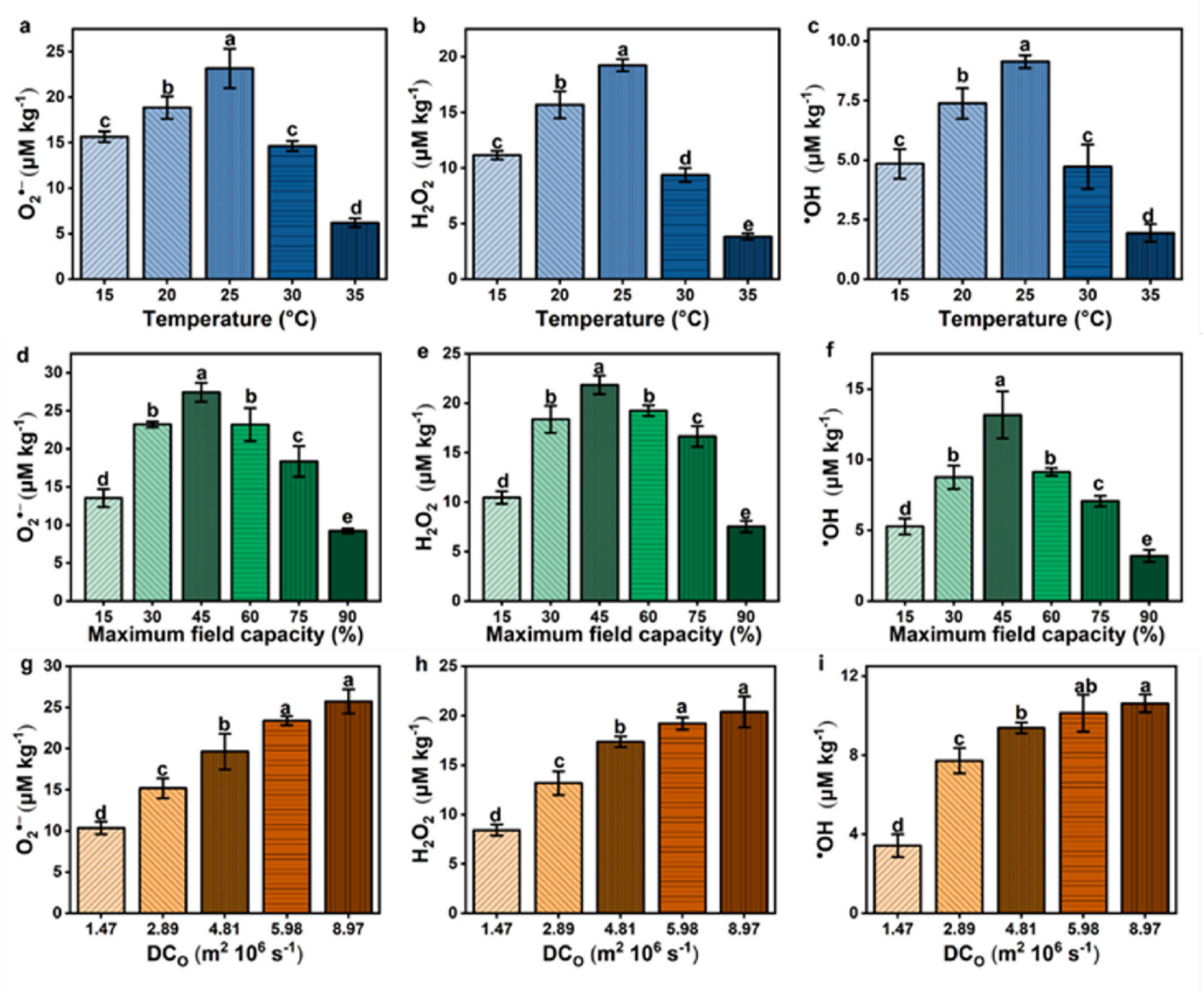

Fig. 2. Effects of different temperatures on the content of (a) $O_2^{\bullet-}$, (b) H_2O_2, and (c) $^{\bullet}$OH in the rhizosphere of maize; Effects of different humidities on the content of (d) $O_2^{\bullet-}$, (e) H_2O_2, and (f) $^{\bullet}$OH in the rhizosphere of maize; Effects of different oxygen availability on the content of (g) $O_2^{\bullet-}$, (h) H_2O_2, and (i) $^{\bullet}$OH in the rhizosphere of maize. DC_o is the diffusivity coefficients of oxygen. The values are presented as the mean ± SD (n = 5), and the error bars represent the standard deviation. Different letters above columns indicate significant differences at $p < 0.05$ level among treatments.

5.63, 4.37 and 5.89 μM kg^{-1}, and 8.37, 7.58 and 7.88 μM kg^{-1}, respectively.

The residual percentages of NAP, PHE, and ANT in the rhizosphere soil decreased from 98.4, 98.9, and 99.4% to 83.1, 63.7, and 50.3%, respectively, after 28 d of maize growth (Fig. S19a), indicating that the maize rhizosphere plays a critical role in PAH transformation. To further determine the potential role of rhizosphere ROS in PAH transformation, scavengers were added to the PAH-contaminated soil before maize planting. The $^{\bullet}$OH and $O_2^{\bullet-}$ contents decreased from 10.56 to 6.65 μM kg^{-1} to 2.45 and 0.91 μM kg^{-1}, respectively, with the addition of *p*-benzoquinone and coumarin (Fig. S3), indicating scavengers could significantly quench $^{\bullet}$OH and $O_2^{\bullet-}$. Moreover, with the addition of *p*-benzoquinone, the residual percentages of NAP, PHE, and ANT increased to 90.1, 76.3, and 71.8%, respectively, after 28 d (Fig. S19b). Similarly, coumarin significantly inhibited NAP, PHE, and ANT removal.

4. Discussion

4.1. Root development effects on rhizosphere ROS generation

Although fixed imaging time and disregarding the time-lapse approach may result in bias in fluorescence imaging (Zhao et al., 2022), the development of rhizosphere ROS could be effectively captured after 1 h incubation (Fig. S2). Fluorescence imaging demonstrated that the maize rhizosphere is a hotspot for ROS production (Fig. 1). Furthermore, with elapsed culture time, the lateral roots, including secondary and tertiary roots, exhibited stronger fluorescence intensity than the seminal roots indicating that higher amounts of ROS accumulated in newly developed roots. In other words, the ROS hotspot gradually shifted from seminal to lateral roots during incubation. In addition, the relatively high proportion of ROS hotspots on day 17 was attributed to the emergence of nodal roots, further demonstrating that root development influences ROS generation and that neonatal roots possess a stronger ability to produce ROS. The evolution of ROS distribution patterns may be related to variations in rhizosphere

characteristics, which are strongly influenced by root development (Fontaine et al., 2007; Blagodatskaya et al., 2009). Compared to seminal roots, lateral roots are generally shorter and smaller during root growth, resulting in different secretory functions (Philippot et al., 2013; Schmidt and Eickhorst, 2014). This can alter root exudate contents and constituents, which play critical roles in stimulating, selecting, and enriching the functional groups of microorganisms, and thus microbial diversity differs over the course of root development (Remenant et al., 2009; Philippot et al., 2013; Tiziani et al., 2020a, 2020b). Similarly, enzymatic activity is influenced by the microbial species and root type (Grierson and Adams, 2000), and enzymatic activity in the rhizosphere may vary owing to root development and interactions with microorganisms. These differences may alter the production, accumulation, and fate of ROS in the rhizosphere.

ROS concentrations, including $O_2^{\bullet-}$, H_2O_2 and $^{\bullet}OH$, significantly changed with root growth (Fig. S5), indicating that root development controls rhizosphere ROS generation. To further investigate how root development regulates rhizosphere ROS production, root exudate evolution, enzymatic activity, and redox components in rhizosphere soil during maize growth were studied and found to be strongly correlated with ROS generation (Page et al., 2014; Zhang et al., 2016a, 2016b). The root exudate quantity, water-soluble phenol content, and enzymatic activity first increased and then decreased with root growth (Figs. S6 and S7c), consistent with the $O_2^{\bullet-}$ and H_2O_2 content trends. Along with cultivation, maize growth was expedited and produced a large amount of root exudates (Fig. S6a), which may have promoted the increase in water-soluble phenol content (Fig. S7c). As previously reported, water-soluble phenols may directly induce O_2 activation, thereby producing $O_2^{\bullet-}$ (Bonke et al., 2021). Meanwhile, an increase in root exudate content may also enhance microbial activity (Chaparro et al., 2014; Li et al., 2014), which could promote enzymatic activity (urease, dehydrogenase, and catalase, Figs. S6b–d) and, in turn, promote biological $O_2^{\bullet-}$ production (Op De Beeck et al., 2018). The $O_2^{\bullet-}$ generated is metastable and is converted into H_2O_2 via dismutation and hydrolysis (Zhang et al., 2016a). Therefore, these plant growth-mediated factors jointly regulate changes in $O_2^{\bullet-}$ and H_2O_2 content. Notably, the changes in the Fe(II) and DOC concentrations aligned with those of the $^{\bullet}OH$ content (Fig. S5c), suggesting that Fe(II) and DOC may mediate $^{\bullet}OH$ production. Correlation analysis revealed a positive correlation between the Fe(II) and DOC contents and $^{\bullet}OH$ production (Fig. S8). In contrast, $O_2^{\bullet-}$ and H_2O_2 generation was significantly correlated with the root exudate and water-soluble phenol contents, and enzymatic activity (Fig. S8). These results further confirm that root development may regulate ROS generation by mediating various factors.

4.2. Environmental condition effects on rhizosphere ROS generation

The $O_2^{\bullet-}$, H_2O_2 and $^{\bullet}OH$ contents first increased and then decreased with temperature, reaching a maximum at 25 °C (Fig. 2a–c). Likewise, maize biomass, particularly stem length, exhibited a trend similar to that of rhizosphere ROS. Previous studies have reported that plant biomass significantly influences biogeochemical processes in the rhizosphere. Sun et al. (2012) found that plant aboveground biomass had an obvious effect on the rhizosphere microbial abundance. In addition, plant photosynthesis and transpiration processes significantly influence the release of root exudates and soil moisture dynamics (Manzoni and Katul, 2014; Tiziani et al., 2020a). Therefore, the effect of temperature on ROS production may be mediated by alterations in the physicochemical and biological properties of the rhizosphere. Specifically, the changes in DOC amount, water-soluble phenol concentration, and root exudate content were consistent with the trend in ROS content (Fig. S12), indicating that temperature may affect rhizosphere ROS generation by regulating these factors. Briefly, both low and high temperatures can exert negative effects on maize growth, with 25 °C being the most favourable temperature for growth (Fig. S9). Under these conditions, the root exudate content reached a maximum, which promoted redox component production (DOC and water-soluble phenols, Figs. S12b–c). As redox-metastable compounds, both could promote the transfer of electrons to oxygen, enhancing $O_2^{\bullet-}$ production (Tong et al., 2016). The $O_2^{\bullet-}$ generated was readily transformed into H_2O_2 and $^{\bullet}OH$ via dismutation (Sinsabaugh, 2010) and Fenton reactions (Diaz et al., 2013; Georgiou et al., 2015), respectively.

Similarly, soil moisture directly influences plant growth, such as biomass and root exudates (Wang et al., 2019), which correlates with rhizosphere physicochemical and biological characteristics (Tiziani et al., 2020a, 2020b), thereby affecting ROS production. Similar to the temperature, the contents of the three types of ROS first increased and then decreased with soil moisture, reaching a maximum at 45% (Fig. 2d–f). Moreover, maize biomass exhibited a trend similar to that of ROS, particularly stem length (Fig. S10). As described above, plant biomass significantly influences rhizosphere biogeochemical properties, and evolution of the amount of DOC, water-soluble phenol content, and root exudate quantity exhibited a similar trend to that of ROS, indicating that soil moisture may also affect rhizosphere ROS generation by regulating these factors.

Differing from temperature and soil moisture, the contents of the three types of ROS gradually increased with the increase in oxygen availability and reached a maximum at 8.97 $m^2\ 10^6\ s^{-1}$ (Fig. 2g–i). In addition, root and stem lengths attained their maximum when DC_o was 4.81 $m^2\ 10^6\ s^{-1}$ (Fig. S11), which differed from the ROS variation trend, indicating that oxygen availability may mediate ROS production through other processes that vary with soil temperature and soil moisture. Moreover, different oxygen availabilities exhibited no obvious differences in the content of root exudates, DOC, water-soluble phenols, and bacterial abundance. These results indicate that the effect of oxygen availability on factors related to ROS production was negligible, and oxygen is more likely to act as a precursor for ROS generation, directly promoting ROS generation (Dai et al., 2022).

As discussed above, environmental conditions not only influenced rhizosphere ROS production but also the chemical and biological properties. Therefore, correlation analysis was performed to explore the pivotal factors regulating ROS production. The three types of ROS under different temperatures and humidities were significantly correlated with the quantities of root exudates, water-soluble phenols, and DOC (Figs. S18a–b), whereas there was no significant relationship with other factors (Fe(II), urease, and bacterial abundance), further indicating that temperature and soil moisture may mediate rhizosphere ROS generation by regulating the changes in root exudate types and amounts, water-soluble phenol concentrations, and DOC content (Liu et al., 2017; Bonke et al., 2021). SEM analysis was conducted to clarify the potential pathways involved in ROS generation in the rhizosphere under various environmental conditions. For rhizosphere ROS generation at different temperatures, SEM explained 91.0, 95.0 and 94.0% of the variance in $O_2^{\bullet-}$, H_2O_2, and $^{\bullet}OH$ generation, respectively, providing a superb fit using the χ^2, RMSE and AIC metrics (Fig. 3a). Similarly, SEM explained 93.0, 94.0, and 92.0% of the variability in $O_2^{\bullet-}$, H_2O_2, and $^{\bullet}OH$ generation, respectively, under different soil moisture conditions (Fig. 3b). These results suggest that temperature and soil moisture can regulate the distribution, composition, and quantity of root exudates, which may affect DOC and water-soluble phenol production, thereby indirectly regulating ROS generation (Bonke et al., 2021). In contrast, under different oxygen availability conditions, ROS production was not correlated with the amount of root exudate, water-soluble phenol concentration, or DOC content, but was positively related to oxygen availability (Fig. 3c), indicating that oxygen directly participates in ROS generation by acting as a precursor (Dai et al., 2022).

4.3. Role of rhizosphere ROS in PAH transformation

The presence of PAHs was accompanied by an increase in rhizosphere ROS, and the promoting effects were PAH molecule-dependent, that is ANT > PHE > NAP (Fig. 4). Previous studies have shown that

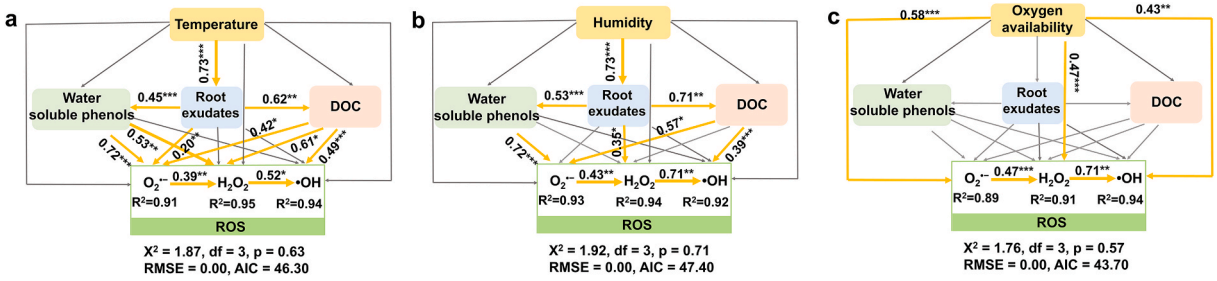

Fig. 3. The effects of root exudates, water-soluble phenols and DOC on ROS production at different temperatures (a), humidities (b) and oxygen availiablities (c). Single-headed arrows indicate the hypothesized direction of causation. As in other linear models, R^2 denotes the proportion of variance explained and appears below every response variable in the model. Model fitness details (χ^2, p, RMSE, and AIC) are close to the figure. Orange and blue solid arrows indicate positive and negative correlation, respectively. Grey arrows indicate insignificant correlation ($p > 0.05$). The arrow width is proportional to the strength of the relationship. The numbers adjacent to the arrows are the standardized path coefficients. *, $p < 0.05$; **, $p < 0.01$; ***, $p < 0.001$.

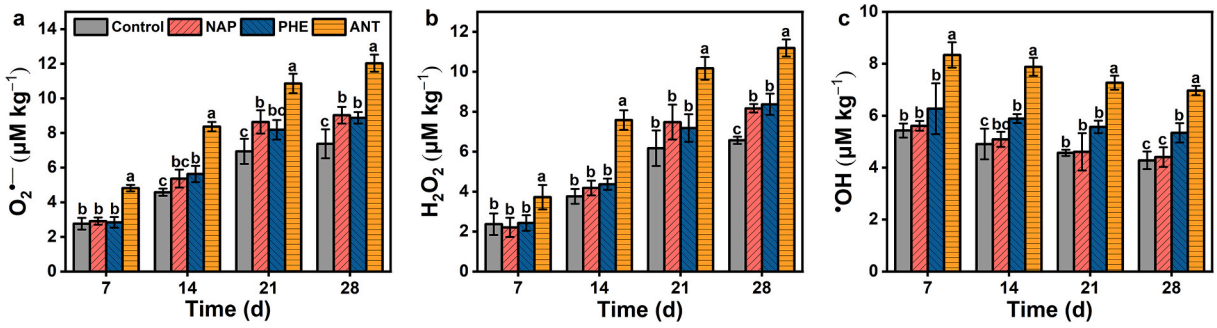

Fig. 4. The change of (a) $O_2^{\bullet-}$, (b) H_2O_2, and (c) $^{\bullet}OH$ in the rhizosphere soil with the growth of maize under the addition of PAHs. The control is the treatment without the addition of PAHs. The NAP, PHE, and ANT are the treatments with the addition of 10 mg kg^{-1} naphthalene, phenanthrene, and anthracene, respectively. The values are presented as the mean ± SD (n = 5), and the error bars represent the standard deviation. Different letters above columns indicate significant differences at $p < 0.05$ level among treatments.

maize can promote the removal of organic pollutants such as PAHs (Yoshitomi and Shann, 2001; Khan et al., 2014). As expected, the PAH residual concentration in the rhizosphere soil decreased with maize growth (Fig. S19a), indicating that the rhizosphere played a critical role in PAH transformation. PAH attenuation in rhizosphere soil is a complex process that involves microbial degradation, plant absorption, formation of non-extractable residues, and abiotic transformation of PAHs mediated by ROS (Harvey et al., 2002; Rivas, 2006; Liu et al., 2023). The attenuation of PAHs was dependent on their molecular characteristics (Fig. S19a), followed by ANT > PHE > NAP. The attenuation efficiency of PAHs exhibited a trend similar to that of ROS generation, indirectly indicating that rhizosphere ROS may play an important role in PAH attenuation. Comparing the differences in PAH residual concentrations before and after the addition of *p*-benzoquinone and coumarin, it was concluded that ROS plays a pivotal role in PAH attenuation in the rhizosphere, with contributions ranging from 31.4 to 43.3%. PAH removal by phytoremediation is generally considered to be associated with biological processes such as microbial degradation, enzymatic transformation, plant accumulation, and plant volatilisation (Lacalle et al., 2018; Hoang et al., 2021). Our results indicate that rhizosphere ROS-mediated abiotic processes play an important but previously unknown role in PAH removal. The pathway for rhizosphere ROS-mediated PAH transformation and the associated mechanisms and strengthening methods are currently unknown. Further investigation at the molecular biology level is required to enhance the potential and application of PAH phytoremediation from the perspective of ROS.

4.4. Environmental implications

To date, ROS production has only been observed in the rhizosphere of rice (Dai et al., 2022) and ryegrass (Liu et al., 2022a). The current study is the first to confirm abundant ROS generation in the maize rhizosphere, which further broadens rhizosphere ROS generation in other plants and indicates that ROS are ubiquitous in the rhizosphere of various plants, including aquatic and terrestrial plants. In addition, the discovery of abundant ROS accumulation in the lateral roots indicated that newly developed roots generally possess the ability to produce ROS and suggested that root structure, exudation release, and rhizodeposition may also have an obvious influence on ROS generation, which requires more delicate methods and scientific experimental designs. Notably, the molecular biology pathway that mediates rhizosphere ROS production is unknown. Further investigations at the genetic and protein levels are required to identify the regulatory networks and key metabolic pathways involved in ROS production in the rhizosphere. The key role of rhizosphere ROS in PAH degradation also reveals a new route for promoting pollutant removal efficiency. The discovery of ROS distribution properties may help us remediate contaminants in specific sites. However, the rhizosphere ROS content changes regularly with temperature, soil moisture, and oxygen availability, which helps optimise environmental conditions for ROS production and thus PAH removal. These results have promising implications for ROS phytoremediation strategies. In addition, our study elucidated the significant effects of environmental conditions on ROS generation in the rhizosphere. Considering the impact of ambient temperature on the promotion of ROS generation and the involvement of ROS in mediating biogeochemical processes, such as organic matter mineralisation (Wu et al., 2023), climate warming may stimulate rhizosphere ROS generation. This further leads to the production of greenhouse gases and thus exacerbates climate change.

5. Conclusion

The current study clearly demonstrated that newly developed roots are pivotal contributors to ROS production. Ambient temperature and soil moisture indirectly influenced ROS production by regulating the release of root exudates to induce changes in water-soluble phenols and DOC, whereas oxygen availability directly mediated ROS generation by acting as a precursor. Furthermore, the presence of PAHs substantially enhances ROS production, which subsequently promotes PAH transformation. These findings deepen our understanding of rhizosphere ROS production under different roots and environmental conditions and provide new insights into the abiotic transformation of PAHs mediated by ROS.

Notes

The authors declare no competing interests.

CRediT authorship contribution statement

Jinbo Liu: Writing – original draft, Visualization, Validation, Software, Methodology, Formal analysis, Data curation, Conceptualization. **Siqi Shen:** Writing – review & editing. **Kecheng Zhu:** Writing – review & editing. **Ziyan Li:** Writing – review & editing. **Na Chen:** Writing – review & editing. **Eric Lichtfouse:** Writing – review & editing. **Hanzhong Jia:** Validation, Supervision, Resources, Project administration, Funding acquisition, Conceptualization.

Declaration of competing interest

The authors declare that they have no known competing financial interests or personal relationships that could have appeared to influence the work reported in this paper.

Data availability

Data will be made available on request.

Acknowledgements

This study was supported by the National Natural Science Foundation of China (Grant No. 42077351), Natural Science Basic Research Program of Shaanxi Province (Grant No. 2024JC-YBQN-0262), and the Shaanxi Science and Technology Plan Project (Grant No. 2024JC-TBZC-05).

Appendix A. Supplementary data

Supplementary data to this article can be found online at https://doi.org/10.1016/j.soilbio.2024.109562.

References

Bonke, S.A., Risse, T., Schnegg, A., Brückner, A., 2021. In situ electron paramagnetic resonance spectroscopy for catalysis. Nature Reviews Methods Primers 33. https://doi.org/10.1038/s43586-021-00031-4.

Blagodatskaya, E.V., Blagodatsky, S.A., Anderson, T.H., Kuzyakov, Y., 2009. Contrasting effects of glucose, living roots and maize straw on microbial growth kinetics and substrate availability in soil. European Journal of Soil Science 60 (2), 186–197. https://doi.org/10.1111/j.1365-2389.2008.01103.x.

Chen, N., Huang, D., Liu, G., Chu, L., Fang, G., Zhu, C., Zhou, D., Gao, J., 2021. Active iron species driven hydroxyl radicals formation in oxygenation of different paddy soils: implications to polycyclic aromatic hydrocarbons degradation. Water Research 203, 117484. https://doi.org/10.1016/j.watres.2021.117484.

Chaparro, J.M., Badri, D.V., Vivanco, J.M., 2014. Rhizosphere microbiome assemblage is affected by plant development. ISME Journal 8 (4), 790–803. https://doi.org/10.1038/ismej.2013.196.

Courchesne, F., Gobran, G.R., 1997. Mineralogical variations of bulk and rhizosphere soils from a Norway spruce stand. Soil Science Society of America Journal 61 (4), 1245–1249. https://doi.org/10.2136/sssaj1997.03615995006100040034x.

Dai, H., Wu, B., Chen, B., Ma, B., Chu, C., 2022. Diel Fluctuation of extracellular reactive oxygen species production in the rhizosphere of rice. Environmental Science & Technology 56 (12), 9075–9082. https://doi.org/10.1021/acs.est.2c00005.

Diaz, J.M., Hansel, C.M., Voelker, B.M., Mendes, C.M., Andeer, P.F., Zhang, T., 2013. Widespread production of extracellular superoxide by heterotrophic bacteria. Science 340 (6137), 1223–1226. https://doi.org/10.1126/science.1237331.

Fu, H., Liu, H., Mao, J., Chu, W., Li, Q., Alvarez, P.J.J., Qu, X., Zhu, D., 2016. Photochemistry of dissolved black carbon released from biochar: reactive oxygen species generation and phototransformation. Environmental Science & Technology 50 (3), 1218–1226. https://doi.org/10.1021/acs.est.5b04314.

Fontaine, S., Barot, S., Barre, P., Bdioui, N., Mary, B., Rumpel, C., 2007. Stability of organic carbon in deep soil layers controlled by fresh carbon supply. Nature 450 (7167), 277. https://doi.org/10.1038/nature06275. U10.

Gunina, A., Kuzyakov, Y., 2015. Sugars in soil and sweets for microorganisms: review of origin, content, composition and fate. Soil Biology and Biochemistry 90, 87–100. https://doi.org/10.1016/j.soilbio.2015.07.021.

Gligorovski, S., Strekowski, R., Barbati, S., Vione, D., 2015. Environmental implications of hydroxyl radicals (•OH). Chemical. Reviews 115 (24), 13051–13092. https://doi.org/10.1021/cr500310b.

Grierson, P.F., Adams, M.A., 2000. Plant species affect acid phosphatase, ergosterol and microbial P in a Jarrah (Eucalyptus marginata Donn ex Sm.) forest in south-western Australia. Soil Biology and Biochemistry 32 (13), 1817–1827. https://doi.org/10.1016/S0038-0717(00)00155-3.

Georgiou, C.D., Sun, H.J., McKay, C.P., Grintzalis, K., Papapostolou, I., Zisimopoulos, D., Panagiotidis, K., Zhang, G., Koutsopoulou, E., Christidis, G.E., Margiolaki, I., 2015. Evidence for photochemical production of reactive oxygen species in desert soils. Nature Communications 6, 7100. https://doi.org/10.1038/ncomms8100.

Guo, H., Liu, S., Wang, Y., Wang, Y., Hou, J., Zhu, T., Liu, Y., 2023. Reduced sulfide and methane in rising main sewer via calcium peroxide dosing: insights from microbial physiological characteristics, metabolisms and community traits. Journal of Hazardous Materials 451, 131138. https://doi.org/10.1016/j.jhazmat.2023.131138.

Guo, H., Tian, L., Wang, Y., Zheng, K., Hou, J., Zhao, Y., Zhu, T., Liu, Y., 2022. Enhanced anaerobic digestion of waste activated sludge with periodate-based pretreatment. Environmental Science and Ecotechnology 13, 100208. https://doi.org/10.1016/j.ese.2022.100208.

Harvey, P.J., Campanella, B.F., Castro, P.M.L., Harms, H., Lichtfouse, E., Schäffner, A.R., Smrcek, S., Werck-Reichharts, D., 2002. Phytoremediation of polyaromatic hydrocarbons, anilines and phenols. Environmental Science and Pollution Research 9 (1), 29–47. https://doi.org/10.1007/BF02987315.

Hayyan, M., Hashim, M.A., AlNashef, I.M., 2016. Superoxide ion: generation and chemical implications. Chemical. Reviews 116 (5), 3029–3085. https://doi.org/10.1021/acs.chemrev.5b00407.

Hoang, S.A., Lamb, D., Seshadri, B., Sarkar, B., Choppala, G., Kirkham, M.B., Bolan, N.S., 2021. Rhizoremediation as a green technology for the remediation of petroleum hydrocarbon-contaminated soils. Journal of Hazardous Materials 401, 123282. https://doi.org/10.1016/j.jhazmat.2020.123282.

Jaeger, C.H., Lindow, S.E., Miller, S., Clark, E., Firestone, M.K., 1999. Mapping of sugar and amino acid availability in soil around roots with bacterial sensors of sucrose and Tryptophan. Applied and Environmental Microbiology 65 (6), 2685–2690. https://doi.org/10.1128/AEM.65.6.2685-2690.1999.

Jia, H., Li, L., Chen, H., Zhao, Y., Li, X., Wang, C., 2015. Exchangeable cations-mediated photodegradation of polycyclic aromatic hydrocarbons (PAHs) on smectite surface under visible light. Journal of Hazardous Materials 287, 16–23. https://doi.org/10.1016/j.jhazmat.2015.01.040.

Kuzyakov, Y., Razavi, B.S., 2019. Rhizosphere size and shape: temporal dynamics and spatial stationarity. Soil Biology and Biochemistry 135, 343–360. https://doi.org/10.1016/j.soilbio.2019.05.011.

Khan, Z., Roman, D., Kintz, T., Alas, M.D., Yap, R., Doty, S., 2014. Degradation, phytoprotection and phytoremediation of phenanthrene by endophyte *Pseudomonas putida*, PD1. Environmental Science & Technology 48 (20), 12221–12228. https://doi.org/10.1021/es503880t.

Liu, J., Zhu, K., Zhang, C., Zhang, X., Chen, N., Jia, H., 2022a. Microscale spatiotemporal variation and generation mechanisms of reactive oxygen species in the rhizosphere of ryegrass: coupled biotic-abiotic processes. Environmental Science & Technology 56 (22), 16483–16493. https://doi.org/10.1021/acs.est.2c06167.

Liu, Y., Evans, S.E., Friesen, M.L., Tiemann, L.K., 2022b. Root exudates shift how N mineralization and N fixation contribute to the plant-available N supply in low fertility soils. Soil Biology and Biochemistry 165, 108541. https://doi.org/10.1016/j.soilbio.2021.108541.

Liu, L., Huang, X., Zhang, J., Cai, Z., Jiang, K., Chang, Y., 2020. Deciphering the relative importance of soil and plant traits on the development of rhizosphere microbial communities. Soil Biology and Biochemistry 148, 107909. https://doi.org/10.1016/j.soilbio.2020.107909.

Lebel, C.P., Ischiropoulos, H., Bondy, S.C., 1992. Evaluation of the probe 2',7'-dichlorofluorescin as an indicator of reactive oxygen species formation and oxidative stress. Chemical Research in Toxicology 5 (2), 227–231. https://doi.org/10.1021/tx00026a012.

Li, X., Rui, J., Mao, Y., Yannarell, A., Mackie, R., 2014. Dynamics of the bacterial community structure in the rhizosphere of a maize cultivar. Soil Biology and Biochemistry 68, 392–401. https://doi.org/10.1016/j.soilbio.2013.10.017.

Liu, X., Cao, L., Wang, Q., Zhang, X., Hu, X., 2017. Effect of tea saponin on phytoremediation of Cd and pyrene in contaminated soils by Lolium multiflorum. Environmental Science and Pollution Research 24 (23), 18946–18952. https://doi.org/10.1007/s11356-017-9515-2.

Liu, J., Zhang, C., Jia, H., Lichtfouse, E., Sharma, V.K., 2023. Abiotic transformation of polycyclic aromatic hydrocarbons via interaction with soil components: a systematic review. Critical Reviews in Environmental Science and Technology 53 (5), 676–699. https://doi.org/10.1080/10643389.2022.2083897.

Lacalle, R.G., Gomez-Sagasti, M.T., Artetxe, U., Garbisu, C., Becerril, J.M., 2018. Brassica napus has a key role in the recovery of the health of soils contaminated with metals and diesel by rhizoremediation. Science of The Total Environment 618, 347–356. https://doi.org/10.1016/j.scitotenv.2017.10.334.

Mopper, K., Zhou, X., 1990. Hydroxyl radical photoproduction in the sea and its potential impact on marine processes. Science 250 (4981), 661–664. https://doi.org/10.1126/science.250.4981.661.

Manning, M.R., Lowe, D.C., Moss, R.C., Bodeker, G.E., Allan, W., 2005. Short-term variations in the oxidizing power of the atmosphere. Nature 436 (7053), 1001–1004. https://doi.org/10.1038/nature03900.

Manzoni, S., Katul, G., 2014. Invariant soil water potential at zero microbial respiration explained by hydrological discontinuity in dry soils. Geophysical Research Letters 41 (20), 7151–7158. https://doi.org/10.1002/2014GL061467.

Nakhaie, D., Kosari, A., Mol, J.M.C., Asselin, E., 2020. Corrosion resistance of hot-dip galvanized steel in simulated soil solution: a factorial design and pit chemistry study. Corrosion Science 164, 108310. https://doi.org/10.1016/j.corsci.2019.108310.

Op De Beeck, M., Troein, C., Peterson, C., Persson, P., Tunlid, A., 2018. Fenton reaction facilitates organic nitrogen acquisition by an ectomycorrhizal fungus. New Phytologist 218 (1), 335–343. https://doi.org/10.1111/nph.14971.

Page, S.E., Kling, G.W., Sander, M., Harrold, K.H., Logan, J.R., McNeill, K., Cory, R.M., 2013. Dark formation of hydroxyl radical in arctic soil and surface waters. Environmental Science & Technology 47 (22), 12860–12867. https://doi.org/10.1021/es4033265.

Philippot, L., Raaijmakers, J.M., Lemanceau, P., van der Putten, W.H., 2013. Going back to the roots: the microbial ecology of the rhizosphere. Nature Reviews Microbiology 11 (11), 789–799. https://doi.org/10.1038/nrmicro3109.

Page, S.E., Logan, J.R., Cory, R.M., McNeill, K., 2014. Evidence for dissolved organic matter as the primary source and sink of photochemically produced hydroxyl radical in arctic surface waters. Environmental Science-Processes & Impacts 16 (4), 807–822. https://doi.org/10.1039/c3em00596h.

Pascual, J.A., Hernandez, T., Garcia, C., Ayuso, M., 1998. Enzymatic activities in an arid soil amended with urban organic wastes: laboratory experiment. Bioresource Technology 64 (2), 131–138. https://doi.org/10.1016/S0960-8524(97)00171-5.

Roe, K.L., Schneider, R.J., Hansel, C.M., Voelker, B.M., 2016. Measurement of dark, particle-generated superoxide and hydrogen peroxide production and decay in the subtropical and temperate North Pacific Ocean. Ocean. Deep-Sea Research Part I-Oceanographic Research Papers 107, 59–69. https://doi.org/10.1016/j.dsr.2015.10.012.

Razavi, B.S., Zarebanadkouki, M., Blagodatskaya, E., Kuzyakov, Y., 2016. Rhizosphere shape of lentil and maize: spatial distribution of enzyme activities. Soil Biology and Biochemistry 96, 229–237. https://doi.org/10.1016/j.soilbio.2016.02.020.

Remenant, B.T., Grundmann, G.L., Jocteur-Monrozier, L., 2009. From the micro-scale to the habitat: assessment of soil bacterial community structure as shown by soil structure directed sampling. Soil Biology and Biochemistry 41 (1), 29–36. https://doi.org/10.1016/j.soilbio.2008.09.005.

Rivas, F.J., 2006. Polycyclic aromatic hydrocarbons sorbed on soils: a short review of chemical oxidation based treatments. Journal of Hazardous Materials 138 (2), 234–251. https://doi.org/10.1016/j.jhazmat.2006.07.048.

Schmidt, H., Eickhorst, T., 2014. Detection and quantification of native microbial populations on soil-grown rice roots by catalyzed reporter deposition fluorescence in situ hybridization. FEMS Microbiology Ecology 87 (2), 390–402. https://doi.org/10.1111/1574-6941.12232.

Shi, K., Liu, Y., Chen, P., Li, Y., 2021. Contribution of lignin peroxidase, manganese peroxidase, and laccase in lignite degradation by mixed white-rot fungi. Waste and Biomass Valorization 12 (7), 3753–3763. https://doi.org/10.1007/s12649-020-01275-z.

Sun, H., Yan, L., Mu, C., 2012. Rhizosphere microbial dynamics of *Leymus chinensis* and its correlation with aboveground biomass and soil environment. African Journal of Microbiology Research 6 (16), 3814–3820. https://doi.org/10.5897/AJMR12.608.

Sinsabaugh, R.L., 2010. Phenol oxidase, peroxidase and organic matter dynamics of soil. Soil Biology and Biochemistry 42 (3), 391–404. https://doi.org/10.1016/j.soilbio.2009.10.014.

Trusiak, A., Treibergs, L.A., Kling, G.W., Cory, R.M., 2018. The role of iron and reactive oxygen species in the production of CO_2 in arctic soil waters. Geochimica et Cosmochimica Acta 224, 80–95. https://doi.org/10.1016/j.gca.2017.12.022, 2018.

Tong, M., Yuan, S., Ma, S., Jin, M., Liu, D., Cheng, D., Liu, X., Gan, Y., Wang, Y., 2016. Production of abundant hydroxyl radicals from oxygenation of subsurface sediments. Environmental Science & Technology 50 (1), 214–221. https://doi.org/10.1021/acs.est.5b04323.

Tiziani, R., Pii, Y., Celletti, S., Cesco, S., Mimmo, T., 2020a. Phosphorus deficiency changes carbon isotope fractionation and triggers exudate reacquisition in tomato plants. Scientific Reports 10 (1), 15970. https://doi.org/10.1038/s41598-020-72904-9.

Tiziani, R., Mimmo, T., Valentinuzzi, F., Pii, Y., Celletti, S., Cesco, S., 2020b. Root handling affects carboxylates exudation and phosphate uptake of white lupin roots. Frontiers in Plant Science 11, 584568. https://doi.org/10.3389/fpls.2020.584568.

Vermilyea, A.W., Dixon, T.C., Voelker, B.M., 2010. Use of $H_2^{18}O_2$ to measure absolute rates of dark H_2O_2 production in freshwater systems. Environmental Science & Technology 44 (8), 3066–3072. https://doi.org/10.1021/es100209h.

Wang, Y., Wu, B., Zheng, X., Chen, B., Chu, C., 2023. Assessing the quantum yield spectrum of photochemically produced reactive intermediates from black carbon of various sources and properties. Water Research 229, 119450. https://doi.org/10.1016/j.watres.2022.119450, 2023.

Wu, M., Wong, G.T.F., Wu, Y.C., Shiah, F.K., Dai, M.H., 2015. Hydrogen peroxide in tropical shelf waters: the northern South China Sea shelf. Deep Sea Research Part II-Topical Studies in Oceanography 117, 143–154. https://doi.org/10.1016/j.dsr2.2015.02.027.

Wardman, P., 1989. Reduction potentials of one-electron couples involving free radicals in aqueous solution. Journal of Physical and Chemical Reference Data 18 (4), 1637–1755. https://doi.org/10.1063/1.555843, 1989.

Wang, C., Fu, B., Zhang, L., Xu, Z., 2019. Soil moisture-plant interactions: an ecohydrological review. Journal of Soils and Sediments 19 (1), 1–9. https://doi.org/10.1007/s11368-018-2167-0.

Wu, P., Xie, M., Clough, T.J., Yuan, D., Wu, S., He, X., Hu, C., Zhou, S., Qin, S., 2023. Biochar-derived persistent free radicals and reactive oxygen species reduce the potential of biochar to mitigate soil N_2O emissions by inhibiting nosZ. Soil Biology and Biochemistry 178, 108970. https://doi.org/10.1016/j.soilbio.2023.108970.

Yan, S., Sun, J., Sha, H., Li, Q., Nie, J., Zou, J., Chu, C., Song, W., 2021. Microheterogeneous distribution of hydroxyl radicals in illuminated dissolved organic matter solutions. Environmental Science & Technology 55 (15), 10524–10533. https://doi.org/10.1021/acs.est.1c03346.

Yu, G.H., Kuzyakov, Y., 2021. Fenton chemistry and reactive oxygen species in soil: abiotic mechanisms of biotic processes, controls and consequences for carbon and nutrient cycling. Earth-Science Reviews 214, 103525. https://doi.org/10.1016/j.earscirev.2021.103525.

Yoshitomi, K.J., Shann, J.R., 2001. Corn (*Zea mays* L.) root exudates and their impact on ^{14}C-pyrene mineralization. Soil Biology and Biochemistry 33 (12–13), 1769–1776. https://doi.org/10.1016/S0038-0717(01)00102-X, 2001.

Zhao, G., Wu, B., Zheng, X., Chen, B., Kappler, A., Chu, C., 2022. Tide-triggered production of reactive oxygen species in coastal soils. Environmental Science & Technology 56 (16), 11888–11896. https://doi.org/10.1021/acs.est.2c03142.

Zheng, X., Wu, B., Zhou, C., Liu, T., Wang, Y., Zhao, G., Chen, B., Chu, C., 2023. Sunlight-driven production of reactive oxygen species from natural iron minerals: quantum yield and wavelength dependence. Environmental Science & Technology 57 (2), 1177–1185. https://doi.org/10.1021/acs.est.2c06942.

Zhang, P., Yuan, S., Liao, P., 2016a. Mechanisms of hydroxyl radical production from abiotic oxidation of pyrite under acidic conditions. Geochimica et Cosmochimica Acta 172, 444–457. https://doi.org/10.1016/j.gca.2015.10.015.

Zhang, T., Hansel, C.M., Voelker, B.M., Lamborg, C.H., 2016b. Extensive dark biological production of reactive oxygen species in brackish and freshwater ponds. Environmental Science & Technology 50 (6), 2983–2993. https://doi.org/10.1021/acs.est.5b03906.

Zhang, N., Bu, X., Li, Y., Zhang, Y., Yuan, S., Wen, Z., Tong, M., Lin, L., 2020. Water table fluctuations regulate hydrogen peroxide production and distribution in unconfined aquifers. Environmental Science & Technology 54 (8), 4942–4951. https://doi.org/10.1021/acs.est.0c00487.

Zhang, P., Yuan, S., 2017. Production of hydroxyl radicals from abiotic oxidation of pyrite by oxygen under circumneutral conditions in the presence of low-molecular-weight organic acids. Geochimica et Cosmochimica Acta 218, 153–166. https://doi.org/10.1016/j.gca.2017.08.032.

Supporting Information

Novel insights into the factors influencing rhizosphere reactive oxygen species production and their role in polycyclic aromatic hydrocarbons transformation

Jinbo Liu[a,b], Shen Siqi[a], Kecheng Zhu[a], Ziyan Li[a], Na Chen[a], Eric Lichtfouse[c], Hanzhong Jia[a] *

[a] Key Laboratory of Low-carbon Green Agriculture in Northwestern China, Ministry of Agriculture and Rural Affairs, College of Natural Resources and Environment, Northwest A&F University, Yangling 712100, China

[b] School of Petroleum Engineering and Environmental Engineering, Yan'an University, Yan'an 716000, China

[c] International Research Center for Renewable Energy, State Key Laboratory of Multiphase Flow in Power Engineering, Xi'an Jiaotong University, Xi'an 710049, China

* Corresponding author E-mails: jiahz@nwafu.edu.cn

Reagents and methods (SI1–SI12), Table S1, and Fig. S1–S19.

SI1 Naphthalene (NAP, 98%), anthracene (ANT, 98%), phenanthrene (PHE, 98%), benzoic acid (BA, 99%), p-hydroxybenzoic acid (*p*-HBA, 98%), vanillic acid (98%) and 1,10-o-phenanthroline (98%) were all supplied by J&K Chemical Ltd. (Beijing, China). 2′,7′-dichlorohydro fluorescein diacetate (DCFH-DA, > 97%) was obtained from Aladdin Biochemical Technology Co., Ltd., Shanghai, China. 2,3-bis(2-methoxy-4-nitro-5-sulfophenyl)-2H-tetrazolium-5-carboxanilide (XTT, 98%) was purchased from Sigma Co. Ltd. (Shanghai, China). Methanol (HPLC grade) and phosphoric acid (H_3PO_4, > 85%, AR) were obtained from Sinopharm Chemical Reagent Co., Ltd. (Shanghai, China). All chemicals were used without further purification.

SI2 The contents of clay, silt and sand were detected using laser particle size analyzer (Mastersizer 2000E). Organic carbon (OC) was measured using the H_2SO_4-$K_2Cr_2O_7$ method. For metal contents, soil samples were completely digested by microwave using the Aqua Regia solution of 3/1 37%HCl/97%HNO_3. Concentration of metal ions in digestion solutions was measured by an inductively coupled plasma atomic emission spectrometer (ICP-AES) from Thermo-ICAP6300, Waltham. For pH determination, a 1/5 w/v mixture of soil in Milli-Q water with soil and solution was placed into a shaker for 1 h, then settled before measuring pH. Cation exchange capacity (CEC) was obtained by adding 0.2 M NH_4Cl to substitute exchangeable cations, such as K^+, Na^+, Ca^{2+}, Mg^{2+}, Al^{3+}, into supernatant from the three consecutive washes, then were analyzed by ICP-AES.

SI3 The various oxygen availability of rhizosphere was set according to the protocol of Nakhaie et al. (2020) (Equation 1):

$$DC_o = 1/N^2 \times (D_{ao} \times Q_a^p + KH \times D_{wo} \times Q_w^p) \quad (1)$$

where DC_o is the effective diffusivity coefficient of oxygen, N is soil porosity, D_{ao} is the free propagation coefficient of oxygen in the air (1.8×10^{-5} m^2 s^{-1} at 20 °C), and D_{wo} is the free propagation coefficient of oxygen in the water (2.2×10^{-9} m^2 s^{-1} at 20 °C). Q_a and Q_w is the proportion of soil pore space filled with air and water, respectively. KH is the Henry equilibrium constant (0.03 at 20 °C). Soil porosity N was calculated as Equation 2:

$$N = 1 - \rho_b/\rho_o \quad (2)$$

where ρ_b is soil bulk density (g cm^{-3}), and ρ_0 is the soil density setted as 2.65 g cm^{-3}. The proportion of soil pore space filled with water Q_w was calculated as Equation 3:

$$Q_w = \rho_b \times w/N \quad (3)$$

where w is the soil moisture content.

SI4 50 g of soil samples were mixed with 25 mL of acetone solution containing 200 mg L^{-1} of PAHs (NAP, ANT, and PHE) in a 250 mL Erlenmeyer flask, and then were shaken for 48 h in a rotary shaker at 70 rpm to make the acetone were completely evaporated and achieve the homogeneity of contaminants. After that, 450 g of air-dried soil was added to the Erlenmeyer flask, and the mixture was mixed to realize the uniform distribution of PAHs in soils, making the initial concentration of PAHs was 10 mg kg^{-1}.

SI5 The residual concentration of PAHs in soils was determined by the method used in our previous study (Jia et al., 2018). Specifically, at pre-selected intervals, the rhizosphere soil was mixed thoroughly and a part of soils were freeze-dried by a model LGJ-10C freeze-dryer (Karaltay Instruments Co., Ltd., Beijing, China) for 24 h. Then, 1 mL solvent mixture of acetone and dichloromethane (v/v = 1/1) was added into 0.05 g (dry weight) soil sample. The suspension was ultrasonicated for 15 min to extract residue PAHs and then centrifuged for 5 min at 20,000 × g to separate the solid from solvents. To ensure the complete extraction of organic compounds from soil samples, the extracting procedure was repeated for three times. Supernatants were collected and filtered using a syringe equipped with a 0.45 μm membrane filter. Finally, the filtrate was placed in amber vial and analyzed for the concentration of PAHs using a high-performance liquid chromatography (HPLC, Thermo Fisher Scientific U3000) equipped with a 25 cm × 4.6 mm, 5 μm Cosmosil C18 column. A sample volume of 10 μL was injected into the HPLC by an autosampler. HPLC conditions were: 85% methanol and 15 % ultrapure water as mobile phase; flow rate of 1 mL min^{-1}; oven temperature 30 °C; UV wavelength of NAP, ANT and PHE at 275, 260 and 240 nm.

SI6 XTT was used to quantify $O_2^{\bullet-}$ based on its reaction with $O_2^{\bullet-}$ to produce XTT formazan (Fu et al., 2016). Briefly, 0.05 g soil samples were mixed with 5 mL 0.05 mM XTT solution and shaken for 24 h under dark condition. Subsequently, the mixture was centrifuged for 5 min at 7000 ×*g*, and the obtained supernatants were collected and filtered using a syringe equipped with a 0.45 μm nylon organic membrane. Finally, the XTT formazan in the filtrate was determined by an Evolution 201 UV-Visible spectrophotometer (Thermo Scientific, USA) at 475 nm (ε = 23,800 M^{-1} cm^{-1}).

H_2O_2 concentration was determined by hydrogen peroxide assay kit purchased from Solarbio Life Sciences Co., Ltd (Beijing, China). Briefly, 0.05 g soil samples were mixed with ultrapure water to achieve a suspension of 10 g/L. After that, the suspension was vortexed for 5 min and then centrifuged for 5 min at 7000 ×*g*. The obtained supernatants were collected and filtered using a syringe equipped with a 0.45 μm nylon water membrane. Finally, the filtrate was utilized for H_2O_2 analysis following the manufacturers' protocol.

Benzoic acid (BA), applied as a chemical probe to quantitatively detect •OH concentration, can react with •OH ($k_{BA,\bullet OH}$ = 5.9 × 10^9 $M^{-1}S^{-1}$) and transformed to *p*-HBA (Zhang and Yuan, 2017). Specifically, 0.05 g soil samples were mixed with 5 mL 10 mM BA solution and shaken for 24 h under dark condition. Subsequently, the mixture was centrifuged for 5 min at 7000 ×g, and the obtained supernatants were collected and filtered using a syringe equipped with a 0.45 μm nylon organic membrane. Finally, the filtrate was placed in amber vial and analyzed for the concentration of p-HBA using a high performance liquid chromatography (HPLC-UV, Thermo Fisher Scientific Ulttimate-3000, USA) equipped with an ultraviolet (UV) detector and an Inter Sustain C18 column (4.6 × 250 mm^2). A sample volume of 20 μL was injected into the HPLC by an autosampler. HPLC conditions were: 85% methanol and 15 % ultrapure water as mobile phase; flow rate of 1 mL min^{-1}; oven temperature 30 °C; UV wavelength of *p*-HBA at 255 nm; total run time was 10 min.

SI7 Fe(II) in the rhizosphere soil was determined by 1,10-o-phenanthroline analytical method (Byrne et al., 2015). Specifically, 0.05 g soil was immersed in 5 mL of 0.1 M HCL and rotated at 200 rpm for 2 h. After that, the mixture was centrifuged at 7000 × g for 10 min, and the supernatant was filtered through a 0.45μm filter membrane. Finally, the concentration of Fe(II) was determined by a 1,10-*o*-phenanthroline analytical method at 510 nm using an

ultraviolet-visible (UV–vis) spectrophotometer (Evolution 201, Thermo).

SI8 The rhizosphere soil was mixed with deionized water at a ratio of 1: 10000 (w/v) and shaken for 24 h. After that, the mixture was centrifuged at 5000 × g for 10 min, and the supernatant was filtered through a 0.45μm filter membrane. Finally, the extract was determined by total organic carbon analyzer (TOC-L, Shimadzu, Japan).

SI9 Water-soluble phenols content was quantified colorimetrically using Folin–Ciocalteau reagent as described by Soleimani et al. (2013) Specifically, 0.05 g rhizosphere soils were extracted by shaking with 25 mL distilled water for 4 h at 100 rpm, followed by centrifugation for 15 min at 5000 rpm. A 10-mL aliquot of extract or standard was placed in a test tube, and 3 mL of Na_2CO_3 solution and 1 mL of Folin-Ciocalteau reagent were added. The solution was mixed well and stand for 1 h at room temperature, and the absorbance of the blue complex formed during this period was determined spectrometrically at 750 nm. Vanillic acid was used as standard, and the amount of phenolic compounds was expressed as vanillin acid equivalents (μg vanillic acid/g soil).

SI10 The root exudates of maize cultivated for different times (i.e., 0, 3, 9, 15, 21 and 33 d) and incubated at different environmental conditions (21 d) were measured according to the previous method proposed by Jiang et al. (2021) with some modification. Specifically, the maize was shaken carefully until the soils detached from roots. After that, the obtained maize was cultured in sterile water for 12 h. The water containing root exudates was freeze-dried to ~10 mL and filtered using a 0.22 μm nylon membrane. Then, the extracts were dried under N_2 gas and then methoximated and trimethylsilylated. The exudates were analyzed by an GC−MS (GCMS-TQ8050 NX, Japan). The capillary column used was a DB-5MS (30 m × 0.25 mm i.d. × 0.25 μm film thickness). The GC injection temperature was 50 °C ramped to 250 °C by 12 °C s^{-1}, and the column temperature was first set at 50 °C for 1 min, then ramped at 20 °C min^{-1} to 330 °C and finally held constant for 5 min. The mass spectrometer was used with unit mass resolution at 17 spectra s^{-1} from 80 to 500 Da at −70 eV ionization energy and 1800 V detector voltage with a 230 °C transfer line and a 250 °C ion source.

SI11

Urease activity: urease activity was measured by the sodium phenate-sodium hypochlorite colorimetric method using urea as the substrate (Guan, 1986). 0.05 g soil samples were placed in a 50 mL Erlenmeyer flask containing 1 mL of toluene, and the mixture was shaken on a mechanical shaker for 15 min. After that, 10% urea solution and 20 mL citrate buffer solution (pH = 6.7) were added to the mixture. The mixture was shaken well and incubated in a 37 °C incubator for 24 h. After incubation, the soil suspension was filtered using quantitative filter paper, and the obtained filtrate (1 mL) were transferred into 50 mL volumetric flask containing 4 mL of 1.35 M sodium phenol solution and 3 mL of 0.9% sodium hypochlorite solution. After reaction for 20 min, ultrapure water was added to the mark of the volumetric flask. Finally, the absorbance of the blue complex formed during this period was determined spectrometrically at 578 nm. Nitrogen standard solution was used as standard, and soil urease activity was expressed as mg NH_4-N/g/24 h.

Dehydrogenase activity: Dehydrogenase activity was analyzed by measuring the reduction of triphenyl-tetrazolium chloride to triphenyl-formazan (Cheema et al., 2009). 0.05 g soil samples were incubated for 24 h at 37 ^oC in 5 mL of 2,3,5-triphenyltetrazolium chloride (TTC) solution. Two drops of concentrated H_2SO_4 were added immediately after the incubation to each sample in order to stop the reaction. The sample was then blended with 5 mL of toluene to extract the reaction product (i.e., TPF) and shaken for 30 min at 250 rpm, followed by centrifugation at 5000 rpm for 5 min and spectrophotometric analysis of absorbance at 492 nm. Soil dehydrogenase activity was expressed as mg TPF /g dry soil/24 h.

Catalase activity: Catalase was assayed as described by Aebi, whereby the activity was determined based on the degradation of H_2O_2 (Aebi, 1984). 0.05 g soil samples were placed in a 100 mL Erlenmeyer flask containing 40 mL distilled water and 5 mL of 0.3% H_2O_2. The mixture was shaken on a mechanical shaker for 20 min. After that, 1 mL saturated aluminum potassium alum solution was added to the mixture immediately. The soil suspension was filtered to a 50 mL Erlenmeyer flask containing 5 mL of 1.5 M H_2SO_4. After filtering, the absorbance of the filter was determined spectrometrically at 240 nm.

SI12 The 16S rDNA gene comprising V3 and V4 regions was amplified by PCR using the primers 341F (5'-CCTACGGGNGGCWGCAG-3') and 805R (5'-GACTACHVGGGTATCTAATCC-3). Samples were sequenced on an Illumina MiSeq platform according to the manufacturer's recommendations, provided by Magigene (Shenzheng, China).

DNA Extraction: DNA from different samples was extracted using the E.Z.N.A.®Stool DNA Kit (D4015, Omega, Inc., USA) according to manufacturer' sinstructions. The reagent which was designed to uncover DNA from trace amounts of sample has been shown to be effective for the preparation of DNA of most bacteria. Nuclear-free water was used for blank. The total DNA was eluted in 50 µL of Elution buffer and stored at -80 °C until measurement in the PCR by Magigene Technology Co., Ltd, Shenzheng, Zhejiang Province, China.

PCR Amplification and 16S rDNA Sequencing. The 5′ ends of the primers were tagged with specific barcods per sample and sequencing universal primers. PCR amplification was performed in a total volume of 25 µL reaction mixtures containing 25 ng of template DNA, 12.5 µL PCR Premix, 2.5 µL of each primer, and PCR-grade water to adjust the volume. The PCR conditions to amplify the prokaryotic 16S fragments consisted of an initial denaturation at 98 °C for 30 seconds; 32cycles of denaturation at 98 °C for 10 seconds, annealing at 54 °C for 30 seconds, and extension at 72 °C for 45seconds; and then final extension at 72 °C for 10 minutes. The PCR products were confirmed with 2% agarose gel electrophoresis. Throughout the DNA extraction process, ultrapure water, instead of a sample solution, was used to exclude the possibility of false-positive PCR results as a negative control. The PCR products were purifyied by AMPure XT beads (Beckman Coulter Genomics, Danvers, MA, USA) and quantified by Qubit (Invitrogen, USA). The amplicon pools were prepared for sequencing and the size and quantity of the amplicon library were assessed on Agilent 2100 Bioanalyzer (Agilent, USA) and with the Library Quantification Kit for Illumina (Kapa Biosciences, Woburn, MA, USA), respectively. The libraries were sequenced on NovaSeq PE250 platform.

Fig. S1. Rhizobox used for the construction of rhizosphere microenvironment.

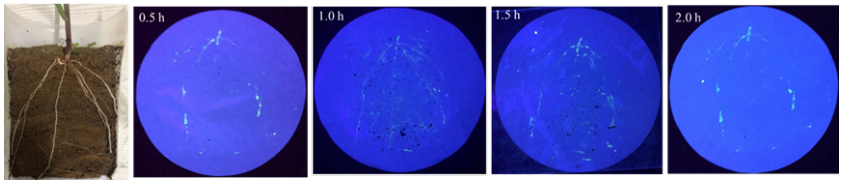

Fig. S2. The evolution of ROS fluorescence imaging with incubation time. After 1 h incubation, the ROS fluorescence intensity was strongest and could effectively show the shape of roots, indicating that 1 h is the optimal incubation time.

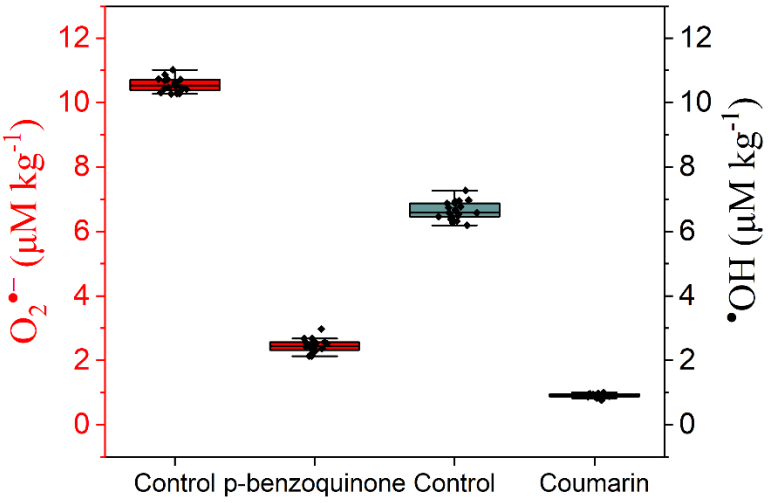

Fig. S3. The quenching effects of *p*-benzoquinone and coumarin on $O_2^{\bullet-}$ and •OH, respectively.

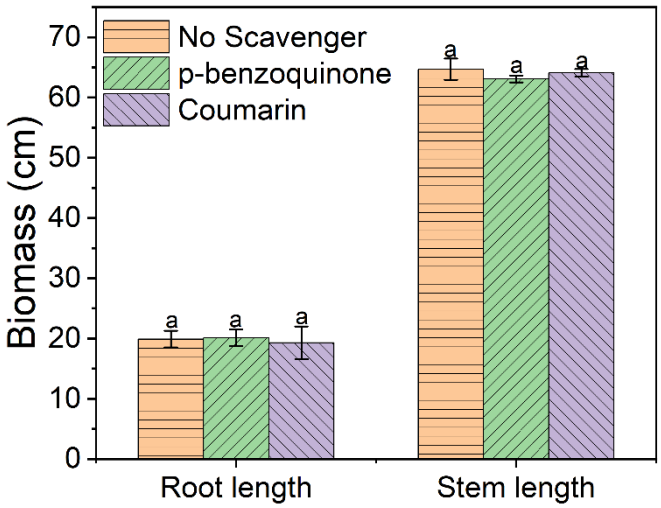

Fig. S4. The influence of *p*-benzoquinone and coumarin on the growth of maize. The values are presented as the mean ± SD (n = 5), and the error bars represent the standard deviation. Different letters above columns indicate significant differences at $p < 0.05$ level among treatments.

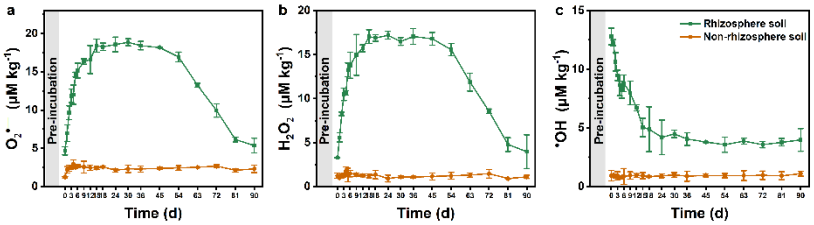

Fig. S5. Evolution of contents of $O_2^{\bullet-}$ (a), H_2O_2 (b), and •OH (c) in the rhizosphere and non-rhizosphere soils with the growth of maize. The values are presented as the mean ± SD (n = 5), and the error bars represent the standard deviation.

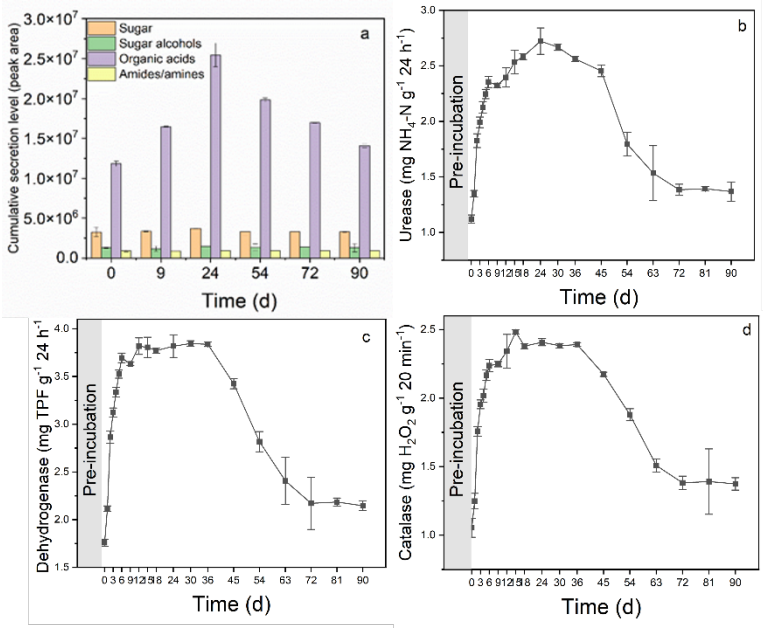

Fig. S6. The cumulative secretion level of compounds (a) and the activity of urease, dehydrogenase, and catalase with the incubation of maize (b-d). The values are presented as the mean ± SD (n = 5), and the error bars represent the standard deviation.

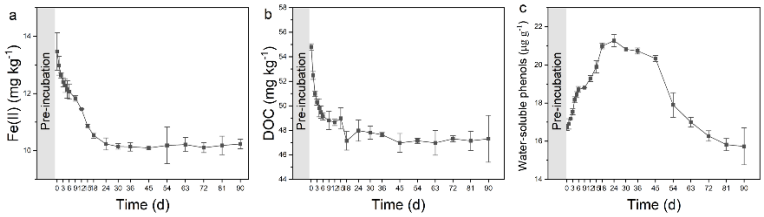

Fig. S7. The evolution of Fe(II) (a), DOC (b) and water-soluble phenols (c) along with the incubation of maize. The values are presented as the mean ± SD (n = 5), and the error bars represent the standard deviation.

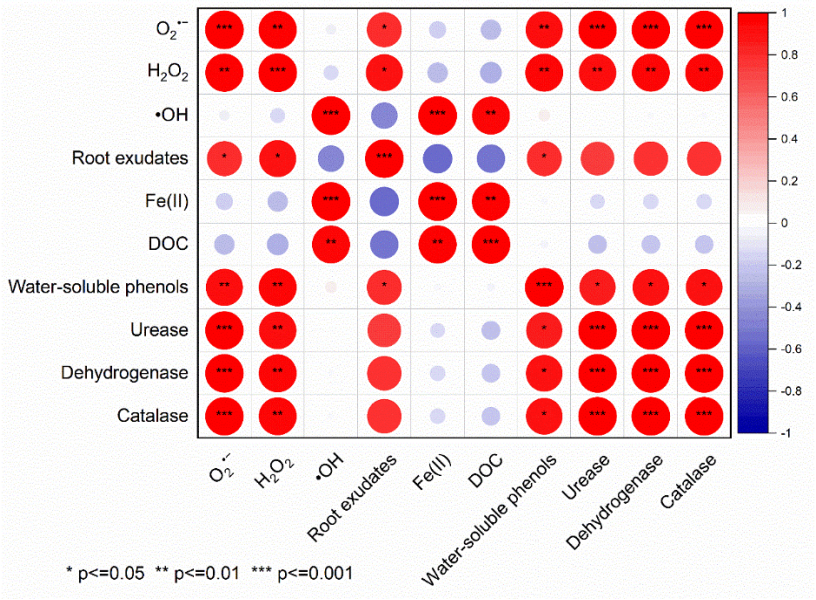

Fig. S8. The correlation analysis among ROS, root exudates, Fe(II), DOC, water-soluble phenols, and enzymes activities.

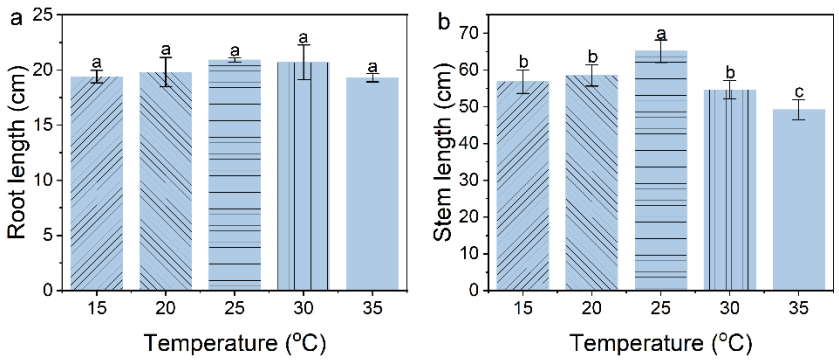

Fig. S9. Effects of different temperatures on (a) root length and (b) stem length of maize. The values are presented as the mean ± SD (n = 5), and the error bars represent the standard deviation. Different letters above columns indicate significant differences at $p < 0.05$ level among treatments.

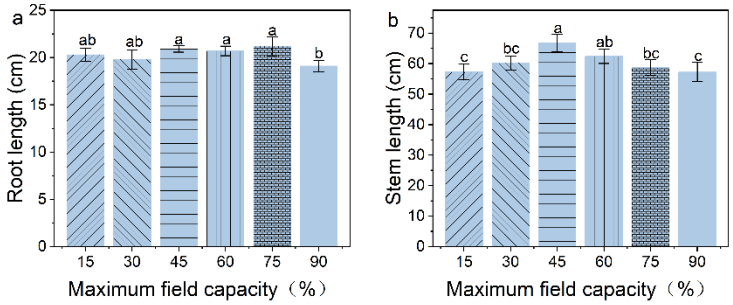

Fig. S10. Effects of different humidities on (a) root length and (b) stem length of maize. The values are presented as the mean ± SD (n = 5), and the error bars represent the standard deviation. Different letters above columns indicate significant differences at $p < 0.05$ level among treatments.

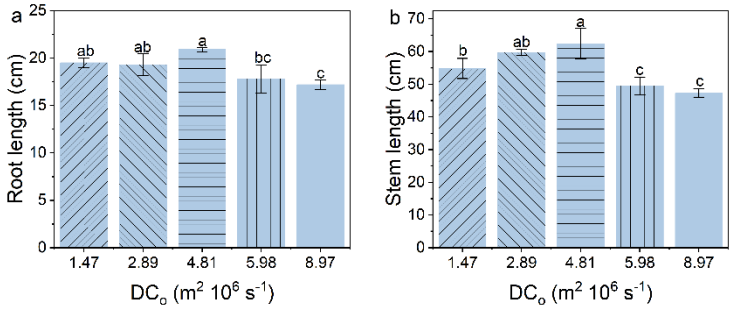

Fig. S11. Effects of different oxygen availabilities on (a) root length and (b) stem length of maize. DC_o is the diffusivity coefficients of oxygen. The values are presented as the mean ± SD (n = 5), and the error bars represent the standard deviation. Different letters above columns indicate significant differences at $p < 0.05$ level among treatments.

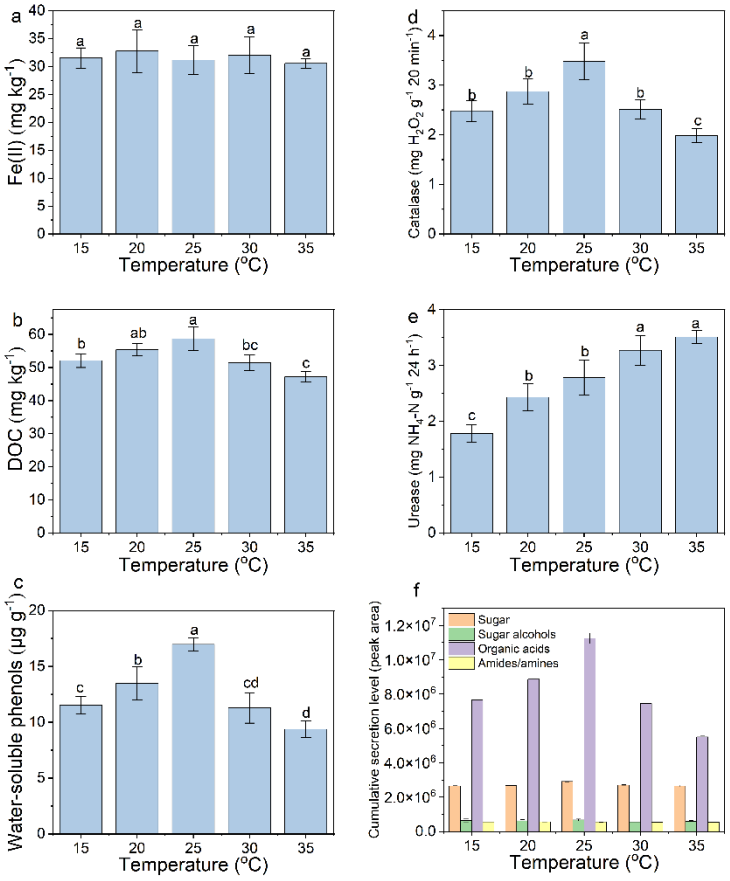

Fig. S12. Effects of different temperatures on (a) Fe(II), (b) DOC, (c) water-soluble phenol, (d) catalase, (e) urease, and (f) root exudates in the rhizosphere of maize. The values are presented as the mean ± SD (n = 5), and the error bars represent the standard deviation. Different letters above columns indicate significant differences at $p < 0.05$ level among treatments.

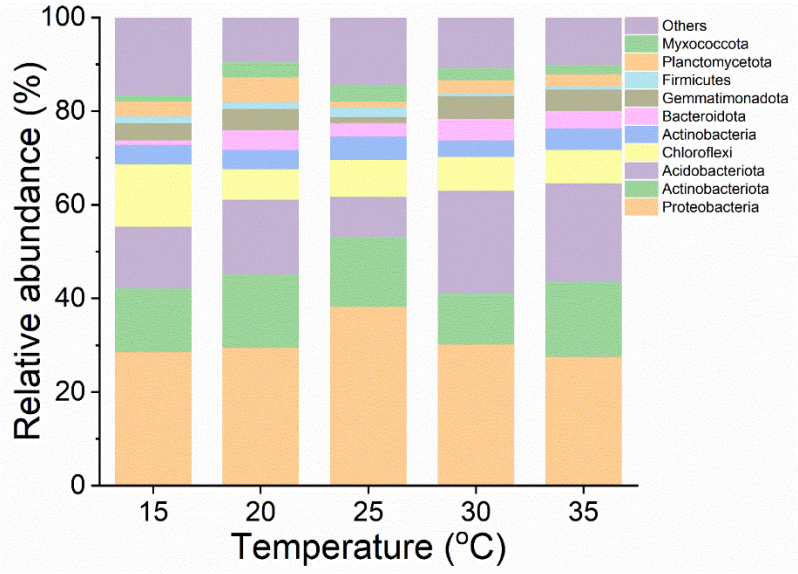

Fig. S13. Relative abundance of soil bacteria at the level of phylum. The relative abundance of bacterial phylum in rhizosphere soil at different temperatures.

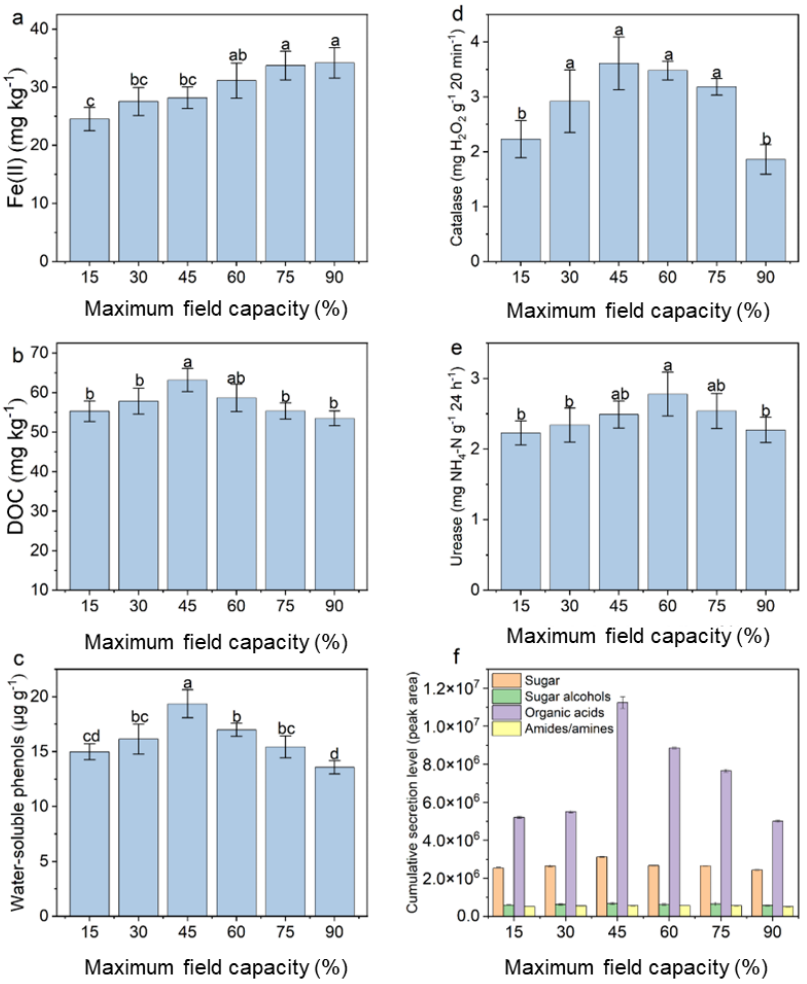

Fig. S14. Effects of different humidities on (a) Fe(II), (b) DOC, (c) water-soluble phenol, (d) catalase, (e) urease, and (f) root exudates in the rhizosphere of maize. The values are presented as the mean ± SD (n = 5), and the error bars represent the standard deviation. Different letters above columns indicate significant differences at $p < 0.05$ level among treatments.

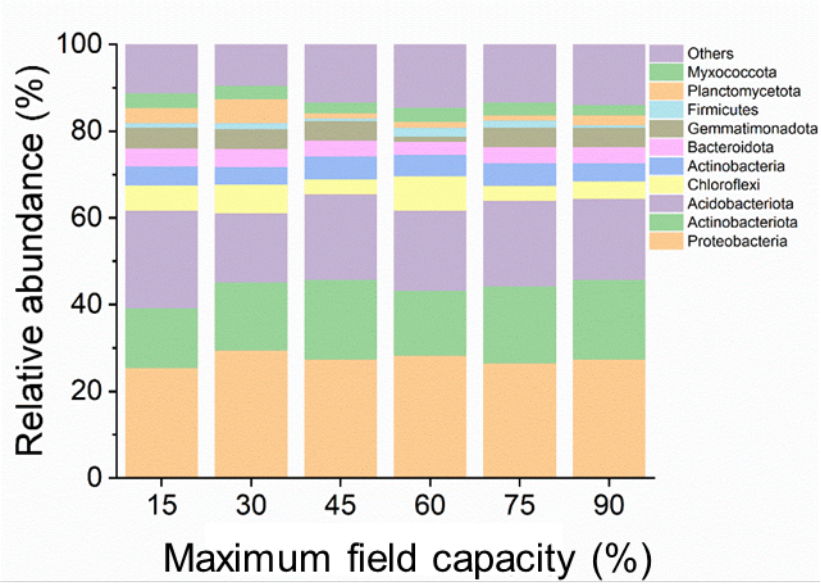

Fig. S15. The relative abundance of bacterial phylum in rhizosphere soil at different humidities.

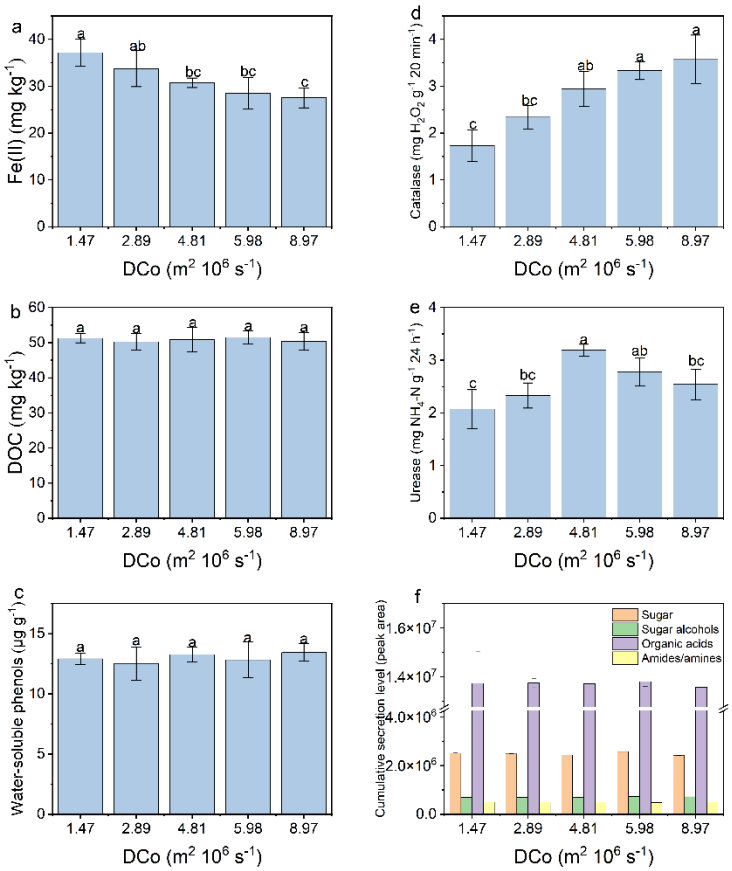

Fig. S16. Effects of different oxygen availabilities on (a) Fe(II), (b) DOC, (c) water-soluble phenol, (d) catalase, (e) urease, and (f) root exudates in the rhizosphere of maize. DC_o is the diffusivity coefficients of oxygen. The values are presented as the mean ± SD (n = 5), and the error bars represent the standard deviation. Different letters above columns indicate significant differences at $p < 0.05$ level among treatments.

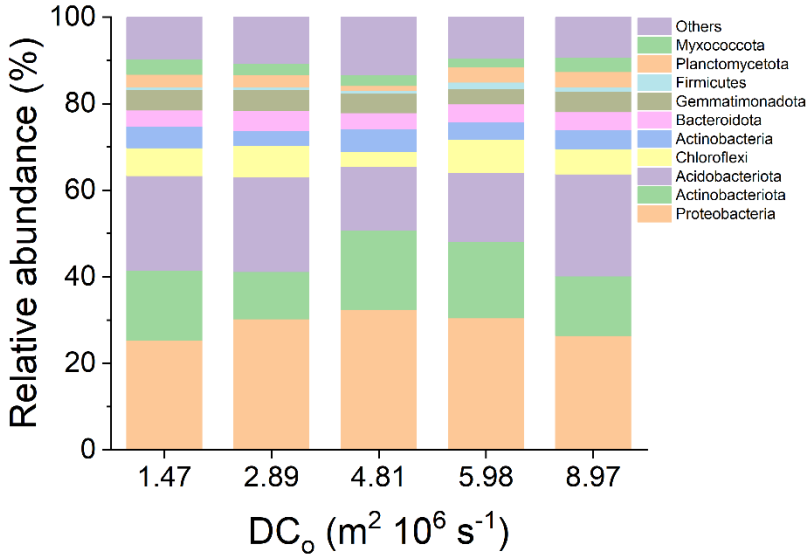

Fig. S17. The relative abundance of bacterial phylum in rhizosphere soil at different oxygen availabilities. DC_o is the diffusivity coefficients of oxygen.

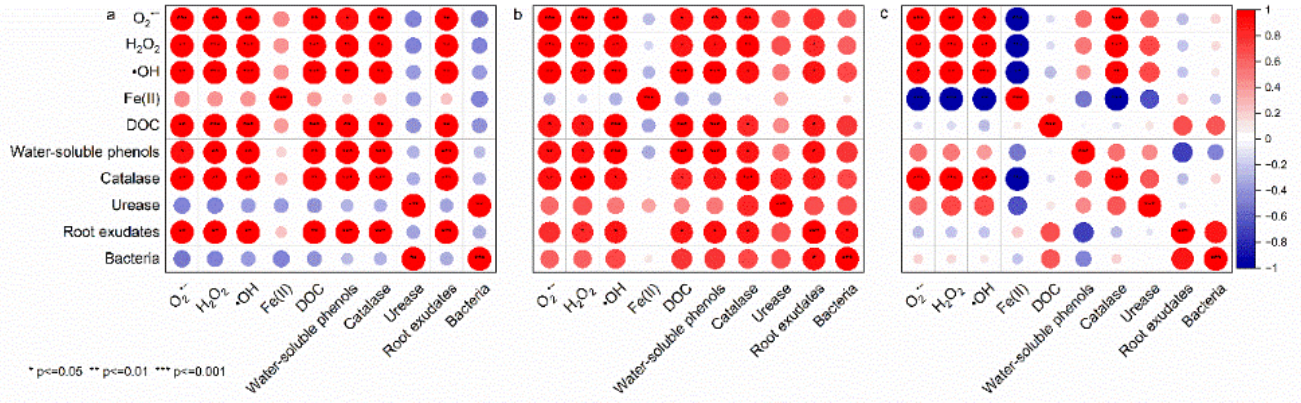

Fig. S18. The correlation analysis among ROS, Fe(II), DOC, water-soluble phenols, enzymes activities, root exudates, and bacterial abundance under different (a) temperatures, (b) humidities and (c) oxygen availabilities.

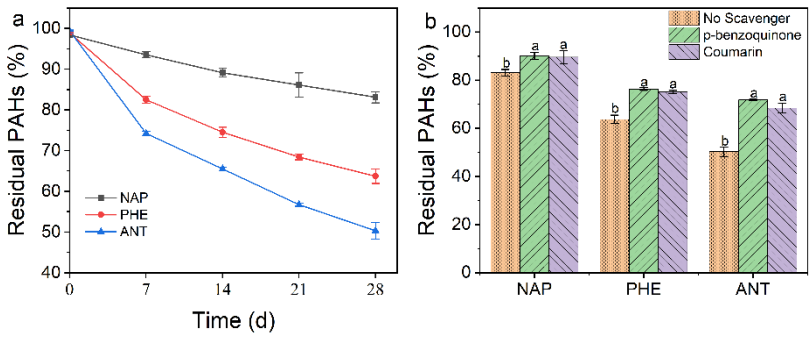

Fig. S19. (a) Temporal evolutions of various PAHs residual percentage and (b) the effects of quenching agent on PAHs residual percentage in maize rhizosphere. The values are presented as the mean ± SD (n = 5), and the error bars represent the standard deviation. Different letters above columns indicate significant differences at $p < 0.05$ level among treatments.

Table S1. The specific settings in the effect of oxygen availability.

Soil weight (g)	ρ_b (g cm^{-3})	DC_o (m^2 10^6 s^{-1})
960	1.28	1.47
945	1.26	2.89
922.5	1.23	4.81
907.5	1.21	5.98
862.5	1.15	8.97

References

Nakhaie, D., Kosari, A., Mol, J.M.C., Asselin, E., 2020. Corrosion resistance of hot-dip galvanized steel in simulated soil solution: A factorial design and pit chemistry study. Corrosion Science 164, 108310. DOI:10.1016/j.corsci.2019.108310.

Jia, H., Zhao, S., Shi, Y., Zhu, L., Wang, C., Sharma, V.K., 2018. Transformation of polycyclic aromatic hydrocarbons and formation of environmentally persistent free radicals on modified montmorillonite: the role of surface metal ions and polycyclic aromatic hydrocarbon molecular properties. Environmental Science & Technology 52 (10), 5725–5733. DOI:10.1021/acs.est.8b00425.

Fu, H., Liu, H., Mao, J., Chu, W., Li, Q., Alvarez, P.J.J., Qu, X., Zhu, D., 2016. Photochemistry of dissolved black carbon released from biochar: reactive oxygen species generation and phototransformation. Environmental Science & Technology 50 (3), 1218–1226. DOI:10.1021/acs.est.5b04314.

Zhang, P., Yuan, S., 2017. Production of hydroxyl radicals from abiotic oxidation of pyrite by oxygen under circumneutral conditions in the presence of low-molecular-weight organic acids. Geochimica et Cosmochimica Acta 218, 153−166. DOI:10.1016/j.gca.2017.08.032.

Byrne, J.M., Klueglein, N., Pearce, C., Rosso, K.M., Appel, E., Kappler, A., 2015. Redox cycling of Fe(II) and Fe(III) in magnetite by Fe-metabolizing bacteria. Science 347 (6229), 1473–1476. DOI:10.1126/science.aaa4834.

Soleimani, M., Farhoudi, M., Christensen, J.H., 2013. Chemometric assessment of enhanced bioremediation of oil contaminated soils. Journal of Hazardous Materials 254, 372−381. DOI:10.1016/j.jhazmat.2013.03.004.

Jiang, L., Luo, C., Zhang, D., Song, M., Mei, W., Sun, Y., Zhang, G., 2021. Shifts in a phenanthrene-degrading microbial community are driven by carbohydrate metabolism selection in a ryegrass rhizosphere. Environmental Science & Technology 55, (2), 962−973. DOI:10.1021/acs.est.0c04951.

Guan, S.Y., 1986. Soil enzymes and soil fertility (in Chinese). Soil Bulletin 41−44. DOI:10.19336/j.cnki.trtb.1980.06.014.

Cheema, S.A., Khan, M.I., Tang, X., Zhang, C., Shen, C., Malik, Z., Ali, S., Yang, J., Shen, K., Chen, X., Chen, Y., 2009. Enhancement of phenanthrene and pyrene degradation in rhizosphere of tall fescue (Festuca arundinacea). Journal of Hazardous Materials 166 (2-3), 1226−1231. DOI:10.1016/j.jhazmat.2008.12.027.

Aebi, H., 1984. Catalase in vitro. Methods in Enzymology 105, 121−126. DOI:10.1016/s0076-6879(84)05016-3